J. Fluid Mech. (2009), *vol.* 622, *pp.* 345–369.
doi:10.1017/S0022112008005259 Printed in the United Kingdom

Asymptotic model for the dynamics of curved viscous fibres with surface tension

NICOLE MARHEINEKE[1]† AND RAIMUND WEGENER[2]

[1]Technische Universität Kaiserslautern, Fachbereich Mathematik, Germany

[2]Fraunhofer-Institut für Techno- und Wirtschaftsmathematik, Kaiserslautern, Germany

(Received 2 December 2007 and in revised form 4 November 2008)

In this paper, we derive and investigate an asymptotic model for the dynamics of curved viscous inertial Newtonian fibres subjected to surface tension, as they occur in rotational spinning processes. Accordingly, we extend the slender body theory of Panda, Marheineke & Wegener (*Math. Meth. Appl. Sci.*, vol. 31, 2008, p. 1153) by including surface tension and deducing boundary conditions for the free end of the fibre. The asymptotic model accounts for the inner viscous transport and places no restrictions on either the motion or the shape of the fibre centreline. Depending on the capillary number, the boundary conditions yield an explicit description for the temporal evolution of the fibre end. We study numerically the behaviour of the fibre as a function of the effects of viscosity, gravity, rotation and surface tension.

1. Introduction

Wallwork *et al.* (2002) presented an asymptotic model for the trajectories of slender curved inviscid jets under surface tension emerging from a rotating orifice, assuming a stationary centreline. In rotational spinning processes of highly viscous fluids, the unrestricted motion of a non-stationary centreline is an important feature that cannot be neglected; a good example is the 'breakup mode 4' in the experiments of Wong *et al.* (2004). Accordingly, the focus of this paper is the systematic asymptotic derivation and numerical investigation of a one-dimensional model that generalizes the work done by Wallwork *et al.* (2002) by allowing for a non-stationary centreline, which is therefore suitable for simulating the spinning of slender curved inertial viscous Newtonian fibres subjected to surface tension. Our approach is to extend the slender body theory of Panda, Marheineke & Wegener (2008) by including surface tension and deducing an asymptotically appropriate boundary condition for the free end of the fibre.

In the process under consideration (see figure 1), a viscous liquid jet leaves a small spinning nozzle located on the curved face of a circular cylindrical drum rotating about its symmetry axis. At the nozzle, the velocity, cross-sectional area and direction of the jet are prescribed. Starting from an initial length of zero, the extruded liquid jet grows and moves due to viscous friction, surface tension and gravity. To describe the process, we choose a coordinate system rotating with the drum. This makes the position of the nozzle and the direction of the inflow time independent, but introduces fictitious rotational body forces due to inertia. The shape of the jet is described by the time-dependent position of its centreline (jet axis), which is defined geometrically as the locus of the mid-points of the cross-sections of the jet and which

† Email address for correspondence: nicole@mathematik.uni-kl.de

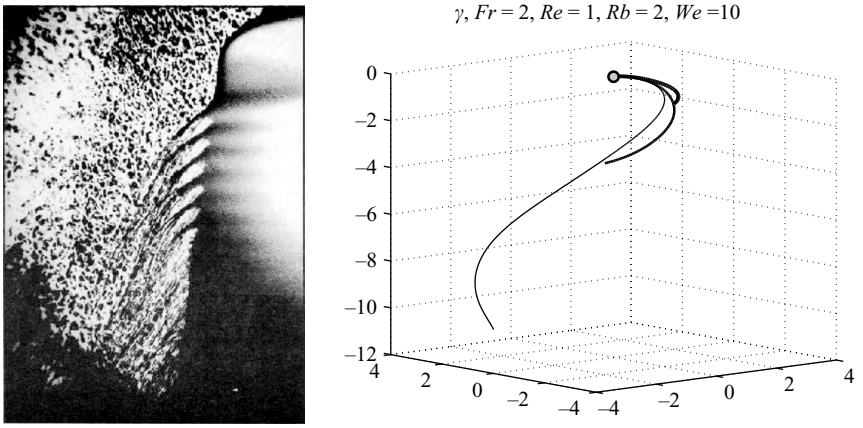

FIGURE 1. (Left) Rotating device used in the production of glass wool (photo by industrial partner). (Right) Centreline $\boldsymbol{\gamma}$ of a viscous fibre extruded from a rotating drum, calculated numerically at dimensionless times $t = 2.5$, 5 and 10 using the method described in this paper.

is, in general, not a streamline of the three-dimensional flow. Our asymptotic model determines the dynamics of the fibre centreline $\boldsymbol{\gamma}(s,t)$, the cross-sectional area $A(s,t)$, the momentum-associated vector-valued velocity $\boldsymbol{v}(s,t)$, the intrinsic scalar-valued velocity $u(s,t)$ and the temporal evolution of the fibre length $L(t)$, where $s \in [0, L(t))$ is the arclength measured from the nozzle and t is the time:

$$\partial_t A + \partial_s(uA) = 0, \tag{1.1a}$$

$$\partial_t(A\boldsymbol{v}) + \partial_s(uA\boldsymbol{v}) = \partial_s\left(\left(\frac{3}{Re}A\partial_s u + \frac{\sqrt{\pi}}{2We}\sqrt{A}\right)\partial_s\boldsymbol{\gamma}\right) + A\boldsymbol{f}, \tag{1.1b}$$

$$\boldsymbol{v} = u\,\partial_s\boldsymbol{\gamma} + \partial_t\boldsymbol{\gamma}, \tag{1.1c}$$

with gravitational and rotational body forces

$$\boldsymbol{f} = \frac{1}{Fr^2}\boldsymbol{e_g} - \frac{2}{Rb}(\boldsymbol{e_\omega} \times \boldsymbol{v}) - \frac{1}{Rb^2}(\boldsymbol{e_\omega} \times (\boldsymbol{e_\omega} \times \boldsymbol{\gamma})) \tag{1.1d}$$

and the boundary conditions

$$\frac{\mathrm{d}L(t)}{\mathrm{d}t} = u(L(t),t), \quad L(0) = 0, \quad (A\partial_s u)(L(t),t) = \frac{\sqrt{\pi}}{6}\frac{Re}{We}\sqrt{A}(L(t),t), \tag{1.1e}$$

$$A(0,t) = 1, \quad u(0,t) = 1, \quad \boldsymbol{\gamma}(0,t) = \boldsymbol{\gamma}_0, \quad \partial_s\boldsymbol{\gamma}(0,t) = \boldsymbol{\tau}_0, \tag{1.1f}$$

at the free fibre end and the nozzle, respectively. Finally, the definition of the arclength parameter implies:

$$\|\partial_s\boldsymbol{\gamma}\| = 1. \tag{1.1g}$$

The variables in (1.1) have been non-dimensionalized using the fluid density, the mean velocity at the nozzle, a typical fibre length and the nozzle area. The dimensionless numbers that appear express the ratios between inertia and viscosity (Reynolds number Re), inertia and surface tension (Weber number We), inertia and gravity (Froude number Fr) and inertia and rotation (Rossby number Rb). The balance laws for mass (cross-section) and momentum are characterized by two velocities $\boldsymbol{v}$ and u that are related by a coupling condition. The momentum-associated velocity $\boldsymbol{v}$ is generated by the geometrical motion of the fibre centreline $\partial_t\boldsymbol{\gamma}$ and the intrinsic velocity u. The intrinsic velocity is the rate of change of the arclength

parameter corresponding to a material point, and is thus related to the inner viscous transport. The balance laws combine the inner viscous transport with the unrestricted motion and shape of the centreline. We use the phrase 'unrestricted motion and shape', since we presuppose a highly non-stationary curved centreline in contrast to previous studies limited to stationary and/or nearly straight fibres. However, to avoid self-penetration of the cross-sections, the condition $R\kappa \leqslant 1$ must hold, where R is the radius of the cross-section and κ is the curvature of the centreline. While the balance laws of the model are certainly physically intuitive, the boundary conditions at the free end require a systematic asymptotic derivation. As we will show, these conditions yield an explicit description for the temporal evolution of $A(L(t), t)$ that involves only on the capillary number $Ca = We/Re$, the ratio of viscous forces and surface tension.

By introducing the convective derivative $\mathrm{D}/\mathrm{D}t = \partial_t + u\partial_s$, our model equations (1.1*a*)–(1.1*c*) can be alternatively written in the primitive variables

$$\begin{aligned}
&\frac{\mathrm{D}}{\mathrm{D}t}A = -A\partial_s u,\\
&\frac{\mathrm{D}}{\mathrm{D}t}\boldsymbol{v} = \frac{1}{A}\partial_s\left(\left(\frac{3}{Re}A\partial_s u + \frac{\sqrt{\pi}}{2We}\sqrt{A}\right)\partial_s\boldsymbol{\gamma}\right) + \boldsymbol{f},\\
&\frac{\mathrm{D}}{\mathrm{D}t}\boldsymbol{\gamma} = \boldsymbol{v},
\end{aligned}$$

which might be easier to interpret physically. However, in this paper we use the conservation form for the underlying three-dimensional problem (2.2) as well as for the asymptotic one-dimensional problem (1.1) because of technical reasons in the model reduction.

The understanding of the dynamics of curved viscous inertial fibres/jets with surface tension under gravity and rotation is of interest in many industrial applications, including the drawing, tapering and spinning of polymer and glass fibres (Pearson 1985, and references therein) and pellet manufacturing (Decent, King & Wallwork 2002; Wallwork *et al.* 2002; Wong *et al.* 2004; Partridge *et al.* 2005). Our work is motivated by the application of glass wool production (figure 1). In rotational spinning processes, hot molten glass is pressed by centrifugal forces through the perforated walls of a rapidly rotating device to form thousands of thin curved liquid fibres. These break up into filaments due to the growth of surface tension-driven instabilities. The filaments cool and solidify while falling down onto a conveyor belt. Numerous theoretical, numerical and experimental investigations have considered various aspects of such processes, including fibre spinning (Pearson 1985; Wallwork *et al.* 2002; Decent *et al.* 2004), breakup and drop formation (Eggers 1997; Stokes, Tuck & Schwartz 2000; Eggers & Dupont 2001; Howell & Siegel 2004; Stokes & Tuck 2004; Wong *et al.* 2004; Partridge *et al.* 2005), dynamics and crystallization of non-Newtonian (viscoelastic) flows (Bechtel *et al.* 1988; Forest & Wang 1994; Forest, Wang & Bechtel 2000), instabilities (Matovich & Pearson 1969; Pearson & Matovich 1969; Shah & Pearson 1972; Geyling & Homsey 1980; Schultz & Davis 1982; Gospodinov & Roussinov 1993; Yarin *et al.* 1999; Forest & Zhou 2001) and the effects of viscosity, surface tension, rotation, gravitation and aerodynamic forces (Entov & Yarin 1984; Dewynne & Wilmott 1993; Cummings & Howell 1999; Wallwork *et al.* 2002; Decent *et al.* 2004; Stokes & Tuck 2004). In this paper, we focus on the systematic asymptotic derivation and numerical investigation of the one-dimensional model (1.1).

For uniaxial flows, one-dimensional models have been widely used to carry out theoretical and numerical stability analysis of glass fibre drawing processes, where the boundary condition at the fibre end is a prescribed pulling velocity (see, e.g. Geyling & Homsey 1980; Gospodinov & Roussinov 1993; Caroselli 1999; Yarin *et al.* 1999; Forest & Zhou 2001). Such models have been heuristically derived with and without surface tension, starting from cross-sectional averaging of the balance laws under certain geometry and profile assumptions (Pearson & Matovich 1969; Pearson 1985; Dewynne, Ockendon & Wilmot 1992 and the references therein). Entov & Yarin (1984), whose model includes linear and angular momentum effects as well as aerodynamic forces, assume that the centreline is nearly straight ($R\kappa \ll 1$ and $R\lambda \ll 1$, where λ is the torsion of the centreline), cross-sections are circular and on the lateral surface the shearing forces vanish and the isotropic normal tractions are small relative to the internal stresses on cross-sections. The first systematic derivation of a one-dimensional fibre model was that of Dewynne *et al.* (1992), which is the basis for several later asymptotic model reduction approaches. These authors used regular asymptotic expansions to simplify the equations describing stationary Stokes flow with a non-stationary free surface, fixed boundaries and no surface tension. Their resulting balance equations are in our dimensionless notation

$$\partial_t A + \partial_s(uA) = 0, \quad \partial_s\left(\frac{3}{Re}A\partial_s u\right) = 0,$$

together with a decoupled hyperbolic evolution equation for the twist of the cross-sections. Their assumption of a nearly straight centreline was extended to a curved dynamic centreline by Howell (1994). At the same time, Dewynne, Howell & Wilmott (1994) deduced an asymptotic fibre model for non-stationary Navier–Stokes flow without surface tension, allowing for a dynamic but nearly straight centreline that is prescribed at the boundaries. This model was subsequently extended to include surface tension by Cummings & Howell (1999). The restriction to nearly straight fibres permits an asymptotic analysis using Cartesian coordinates. Numerical investigations of Stokes and Navier–Stokes flows in straight fibres without surface tension can be found, e.g. in the context of honey dripping under gravity (Stokes *et al.* 2000, Stokes & Tuck 2004).

For flows involving curved and coiled fibres, such as those that interest us here, the studies of Decent *et al.* (2002); Wallwork *et al.* (2002); Decent *et al.* (2004); Ribe (2004) and Ribe, Habibi & Bonn (2006*a*) are certainly central and worth pointing out. As already mentioned, the former studies involve numerical simulation of inviscid (Decent *et al.* 2002) and viscous (Decent *et al.* 2004) liquid jets emerging from a rotating orifice in prilling processes for which a linear stability analysis has been developed in Wallwork *et al.* (2002). The asymptotic approach presupposes a stationary centreline as well as circular cross-sections and constant velocity profiles at leading order. The curved centreline is handled by a covariant coordinate transformation. For the steady coiling of viscous jets without surface tension, Ribe (2004) proposed an asymptotic analysis based on the cross-sectionally averaged linear and angular momentum equations, assuming a stationary and moderately curved ($R\kappa \ll 1$) centreline. Including bending, twisting as well as stretching the model was extended to a dynamic centreline in Ribe, Habibi & Bonn (2006*a*).

Most of the uniaxial models, as well as the stationary model with a curved centreline of Decent and Wallwork, are special cases of the curved non-stationary model without surface tension that we presented recently in Panda *et al.* (2008). Based on the previously developed methodologies, in that work we derived systematically an

asymptotic fibre model without any restriction on the centreline motion and shape (i.e. $R\kappa \leqslant 1$), cross-sectional shape, profile quantities or the inner viscous transport. To handle the nonlinearity and the curved geometry, we used a formulation of the Navier–Stokes equations in scaled curvilinear coordinates that involves two velocities $\boldsymbol{u}$ and $\boldsymbol{v}$, where $\boldsymbol{u}$ describes the convection in the chosen curvilinear coordinates and $\boldsymbol{v}$ the actual velocity in the underlying spatial coordinates. However, the neglect of surface tension in Panda *et al.* (2008) suppresses important effects such as drop formation and rupture that are caused by surface-tension-driven instabilities (see Eggers & Dupont 2001; Sierou & Lister 2003; Wong *et al.* 2004; Partridge *et al.* 2005). Accordingly, the aim of this paper is to extend the slender body theory of Panda *et al.* (2008) to include surface tension, and in particular to deduce asymptotically appropriate boundary conditions for the free end of the fibre. To date, only heuristic boundary conditions have been suggested, e.g. in Eggers & Dupont (2001). In the terminology of Antman (2006), our model (1.1) is a 'string' model consisting of balance equations for mass and linear momentum. They coincide with those of Entov & Yarin (1984) (see the Appendix for details concerning the definition of the different velocities used in the literature). Decoupled from the string part, Entov & Yarin (1984) stated an additional equation for the angular momentum that might be incorporated in our model using asymptotic expansions to higher order. By the choice of a non-stationary material centreline as reference curve in contrast to our geometrical one, the approach in Ribe (2004) and Ribe *et al.* (2006*a*) turns out to be a 'rod' model with fully coupled equations for mass, linear and angular momentum. Especially the coupling of the twisting with the motion of the centreline is very important for the coiling of a fibre falling on a rigid substrate, but not so relevant for the rotational spinning of a fibre whose end is free. 'String' and 'rod' model coincide in case of negligibly small internal shearing forces. The numerical analysis of our model shows a realistic fibre behaviour due to the effects of viscosity, gravity, rotation and surface tension that compares favourably with the experimental data of Wong *et al.* (2004).

The three-dimensional free boundary value problem (BVP) for the spinning of a slender curved inertial viscous fibre is characterized by the slenderness parameter ϵ, i.e. ratio between nozzle width and typical fibre length, which enters the problem via the inflow and the dynamic boundary conditions due to the definition of the Weber number. Applying the transformation theory of Panda *et al.* (2008) and formulating the free BVP in scaled curvilinear coordinates with respect to the fibre centreline and the slenderness parameter in § 2, we embed the BVP into a fibre family whose inflow conditions are independent of ϵ. Their asymptotic analysis follows the spirit of Dewynne *et al.* (1992) by using standard expansion techniques in powers of the slenderness parameter for the model reduction. We thereby determine the (*a priori* unknown) relation between the cross-sectional areas and their boundaries by the assumption of circular cross-sections. Finally, the comparison of the volume-averaged three-dimensional balance laws with the line-averaged one-dimensional balance laws yields the appropriate boundary conditions for the free end of the fibre. The resulting one-dimensional model can be understood as a generalization of existing models to the case of unrestricted motion of a viscous fibre with an arbitrarily curved centreline and surface tension. The effects of viscosity, gravity, rotation and surface tension on the fibre dynamics are numerically investigated in § 3 by applying a finite-volume method on a staggered grid with an implicit upwind flux discretization. We focus on analysing the motion of the fibre centreline and the temporal evolution of the fibre end, and discuss the range of validity of our model with respect to the given parameters.

2. Asymptotic derivation

2.1. *Three-dimensional free boundary value problem*

We model the spinning of a slender curved viscous fibre as a three-dimensional free BVP for an incompressible Newtonian fluid with surface tension. For simplicity, we neglect the temperature dependence of all physical properties. The boundary of the flow domain $\Omega^\star(t) \subset \mathbb{R}^3$ consists of the time-independent inlet $\Gamma_{in}^\star$ representing the nozzle and the time-dependent free surface $\Gamma_{fr}^\star(t)$. We non-dimensionalize the underlying Navier–Stokes equations using the fluid density ρ, the mean velocity V at the spinning nozzle and a typical fibre length ℓ for the spinning process considered. The small ratio between the nozzle width and the length ℓ is the slenderness parameter ϵ. Hence, due to the scaling with V, the dimensionless inflow velocity profile $\boldsymbol{v}_{in}$ at the nozzle satisfies

$$|\Gamma_{in}^\star|^{1/2} = \epsilon \ll 1, \quad \int_{\Gamma_{in}^\star} \boldsymbol{v}_{in} \cdot \boldsymbol{\tau}_0 \, \mathrm{d}\mathscr{A} = \epsilon^2, \tag{2.1}$$

where $|\Gamma_{in}^\star| = \int_{\Gamma_{in}^\star} \mathrm{d}\mathscr{A}$ denotes the measure of the planar cross-sectional area of the nozzle $\Gamma_{in}^\star$ and $\boldsymbol{\tau}_0$ denotes its inward-directed normal vector. The spinning process is characterized by the dimensionless Reynolds number $Re = \ell\rho V/\mu$ and Weber number $We = (\epsilon\ell/2)\rho V^2/\sigma$, where μ is the dynamic viscosity and σ is the coefficient of surface tension. The effective length $\epsilon\ell/2$ that appears in the definition of the Weber number can be understood as the typical radius of curvature of the free surface.

The balance laws for mass and momentum in the flow domain $\Omega^\star(t)$ are now,

$$\nabla_{\boldsymbol{r}} \cdot \boldsymbol{v} = 0, \tag{2.2a}$$

$$\partial_t \boldsymbol{v} + \nabla_{\boldsymbol{r}} \cdot (\boldsymbol{v} \otimes \boldsymbol{v}) = \nabla_{\boldsymbol{r}} \cdot \boldsymbol{T}^T + \boldsymbol{f} \quad \text{with} \quad \boldsymbol{T} = -p\,\boldsymbol{I} + \frac{1}{Re}(\nabla_{\boldsymbol{r}}\boldsymbol{v} + (\nabla_{\boldsymbol{r}}\boldsymbol{v})^T), \tag{2.2b}$$

and the kinematic and dynamic boundary conditions for the free surface $\Gamma_{fr}^\star(t)$ are

$$(\boldsymbol{v} \cdot \boldsymbol{n}^\star) = w^\star, \quad (\boldsymbol{T} \cdot \boldsymbol{n}^\star) = -\frac{\epsilon}{We}(H\boldsymbol{n}^\star). \tag{2.2c}$$

As mentioned, we prescribe the inflow velocity profile $\boldsymbol{v}_{in}$ at the nozzle $\Gamma_{in}^\star$ and initialize the spinning process with an empty flow domain $\Omega^\star(0) = \emptyset$. The unknowns of the BVP (2.2) are the field variables for velocity $\boldsymbol{v}$ and pressure p as well as the flow domain $\Omega^\star(t)$ itself, which is determined by the unit outer normal vectors $\boldsymbol{n}^\star$ and the scalar speed $w^\star$ of its free surface $\Gamma_{fr}^\star(t)$. The jump in the normal stresses at $\Gamma_{fr}^\star(t)$ is incorporated in the definition of the Newtonian stress tensor $\boldsymbol{T}$ by choosing p as the hydrodynamic pressure relative to a constant atmospheric pressure. The effects of surface tension are represented by the inhomogeneous dynamic boundary condition for $\boldsymbol{T}$ with a mean curvature H that is deduced from the geometry. The model is completed by the choice of appropriate body forces $\boldsymbol{f}$, which in our case include gravitational and rotational forces.

The slenderness parameter ϵ enters the spinning problem via the inflow domain $\Gamma_{in}^\star$ in (2.1). For the reduction to an asymptotic one-dimensional model, we follow the concept of Panda *et al.* (2008) and formulate (2.2) in appropriate scaled curvilinear coordinates. To emphasize the analogy between geometrical quantities in the curvilinear coordinates and those in the spatial problem, we use the same notation but suppress the superscript *. The idea behind the introduction of these coordinates is to provide an inflow domain Γ_{in} that is independent of ϵ. The corresponding balance laws are ϵ dependent and form the basis for the rest of

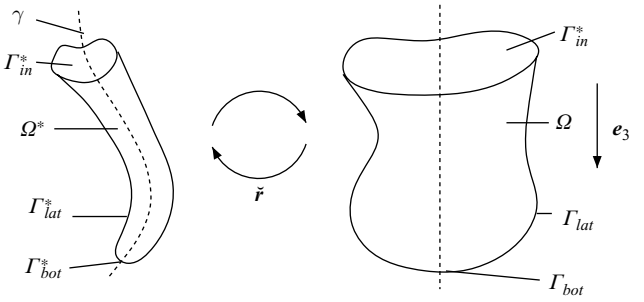

FIGURE 2. Fibre domain in spatial (left) and in scaled curvilinear coordinates (right).

the asymptotic derivation. Concretely, we define a bijective time-dependent scaled curvilinear coordinate transformation $\check{\boldsymbol{r}} : \Omega(t) \to \Omega^\star(t)$,

$$\check{\boldsymbol{r}}(\boldsymbol{x}, t) = \boldsymbol{\gamma}(s, t) + \epsilon\, x_1 \boldsymbol{\eta}_1(s, t) + \epsilon\, x_2 \boldsymbol{\eta}_2(s, t), \quad \text{with} \quad s = x_3, \tag{2.3}$$

with respect to the slenderness parameter ϵ and an arclength parameterized curve $\boldsymbol{\gamma}(s, t)$ with $s \in [0, L(t))$, i.e. $\|\partial_s \boldsymbol{\gamma}\| = 1$. We identify this curve as the centreline of length $L(t)$ of our flow domain $\Omega^\star(t)$ (cf. figure 2). Assuming sufficient regularity of $\boldsymbol{\gamma}$, the curvature $\kappa = \|\partial_{ss}\boldsymbol{\gamma}\|$, $\kappa \neq 0$ and the torsion $\lambda = \partial_s \boldsymbol{\gamma} \cdot (\partial_{ss}\boldsymbol{\gamma} \times \partial_{sss}\boldsymbol{\gamma})/\kappa^2$ are well defined. The vectors $\boldsymbol{\eta}_1$ and $\boldsymbol{\eta}_2$ together with the tangent $\boldsymbol{\tau}$ of $\boldsymbol{\gamma}$ constitute a local orthonormal basis along the curve. They can be written in the forms:

$$\boldsymbol{\tau} = \partial_s \boldsymbol{\gamma}, \quad \boldsymbol{\eta}_1 = \cos\phi\, \boldsymbol{\eta} - \sin\phi\, \boldsymbol{b}, \quad \boldsymbol{\eta}_2 = \sin\phi\, \boldsymbol{\eta} + \cos\phi\, \boldsymbol{b},$$

where $\boldsymbol{\eta} = \partial_{ss}\boldsymbol{\gamma}/\kappa$ and $\boldsymbol{b} = \boldsymbol{\tau} \times \boldsymbol{\eta}$ denote the normal and binormal vectors, respectively, and $\phi(s, t) = \int_0^s \lambda(\sigma, t)\, \mathrm{d}\sigma$ is the torsion angle (see Bishop 1975). According to the Serret–Frenet formulae, the basis vectors satisfy,

$$\partial_s \boldsymbol{\tau} = (\partial_\alpha h)\boldsymbol{\eta}_\alpha, \quad \partial_s \boldsymbol{\eta}_\alpha = -(\partial_\alpha h)\boldsymbol{\tau} \quad \text{with } h(\boldsymbol{x}, t) = x_1\kappa\cos\phi + x_2\kappa\sin\phi, \ \alpha = 1, 2.$$

Here and henceforth, we apply a generalized Einstein summation convention wherein Greek indices range over the values $\{1, 2\}$. We specify the flow domain $\Omega^\star(t)$ in terms of the corresponding domain $\Omega(t)$ in the coordinates, i.e. $\Omega^\star(t) = \check{\boldsymbol{r}}(\Omega(t), t)$. Therefore, we assume $\Omega(t)$ to be composed of cross-sections $\mathscr{A}(s, t)$ that we characterize by a smooth 2π-periodic non-negative radius function $R(\psi, s, t)$

$$\Omega(t) = \cup_{s\in[0,L(t))} \mathscr{A}(s, t) \times \{s\}, \tag{2.4}$$

$$\mathscr{A}(s, t) = \{(x_1, x_2) \in \mathbb{R}^2 \,|\, (x_1, x_2) = (\varrho\cos\psi, \varrho\sin\psi), \varrho \in [0, R(\psi, s, t)], \ \psi \in [0, 2\pi)\}.$$

By this geometrical assumption (2.4) on the flow domain we admit all essential fibre motions of interest in spite of limiting the general fibre behaviour in the considered rotational spinning processes. Here, the bijectivity of the coordinate transformation (2.3) is the crucial constraint, which is violated if $R\kappa > 1$. However, this condition is evidently weaker than the assumption $R\kappa \ll 1$ used, e.g. in Entov & Yarin (1984) and Ribe (2004). Summing up, the whole fibre domain is described by three quantities: the fibre length L, the radius function R and the fibre curve $\boldsymbol{\gamma}$. The identification of $\boldsymbol{\gamma}$ with the centreline implies that

$$\int_{\mathscr{A}(s,t)} x_1\, \mathrm{d}x_1\, \mathrm{d}x_2 = \int_{\mathscr{A}(s,t)} x_2\, \mathrm{d}x_1\, \mathrm{d}x_2 = 0, \tag{2.5}$$

in the curvilinear coordinates. Moreover, the centreline satisfies $\boldsymbol{\gamma}(0, t) = \boldsymbol{\gamma}_0$ as well as $\partial_s \boldsymbol{\gamma}(0, t) = \boldsymbol{\tau}_0$ in accordance with our geometrical assumption, since we consider the

spatial inflow boundary $\Gamma_{in}^{\star}$ to be planar with centre point $\boldsymbol{\gamma}_0$ and inward-directed normal $\boldsymbol{\tau}_0$. Accordingly, the ϵ-independent relations for inflow velocity profile and slenderness parameter stemming from (2.1) are as follows:

$$|\Gamma_{in}| = |\mathscr{A}|(0,t) = 1, \quad \int_{\Gamma_{in}} \boldsymbol{v}_{in} \cdot \boldsymbol{\tau}_0 \, \mathrm{d}\mathscr{A} = \int_{\mathscr{A}(0,t)} \boldsymbol{v}_{in} \cdot \boldsymbol{\tau}_0 \, \mathrm{d}x_1 \, \mathrm{d}x_2 = 1. \tag{2.6}$$

As shown in figure 2, our fibre has a bottom surface that might – but need not – shrink to a single point ($|\mathscr{A}(L(t),t)| = |\Gamma_{bot}(t)| = 0$) due to the action of surface tension. We therefore distinguish between the lateral and the bottom portions of the free surface in the curvilinear coordinates, i.e. $\Gamma_{fr}(t) = \Gamma_{lat}(t) \cup \Gamma_{bot}(t)$, $\Gamma_{lat}(t) \cap \Gamma_{bot}(t) = \emptyset$. The lateral surface $\Gamma_{lat}(t)$ can be parameterized by the bijective function $\boldsymbol{\xi}(\cdot, t)$ for a fixed time t, defined as

$$\boldsymbol{\xi}(\psi, s, t) = R(\psi, s, t)\cos\psi \, \boldsymbol{e}_1 + R(\psi, s, t)\sin\psi \, \boldsymbol{e}_2 + s\boldsymbol{e}_3,$$

with canonical basis $\{\boldsymbol{e}_i\}$, $i = 1, 2, 3$ in $\mathbb{R}^3$. The corresponding outward-directed normal vector $\boldsymbol{n}$ and surface speed w are then given by

$$\boldsymbol{n}(\boldsymbol{\xi}, t) = \frac{\partial_\psi \boldsymbol{\xi} \times \partial_s \boldsymbol{\xi}}{\|\partial_\psi \boldsymbol{\xi} \times \partial_s \boldsymbol{\xi}\|} = \frac{\partial_\psi (R\sin\psi)\boldsymbol{e}_1 - \partial_\psi (R\cos\psi)\boldsymbol{e}_2 - R\partial_s R \boldsymbol{e}_3}{\sqrt{R^2 + (\partial_\psi R)^2 + R^2(\partial_s R)^2}},$$

$$w(\boldsymbol{\xi}, t) = \partial_t \boldsymbol{\xi} \cdot \boldsymbol{n}(\boldsymbol{\xi}, t) = \frac{R\partial_t R}{\sqrt{R^2 + (\partial_\psi R)^2 + R^2(\partial_s R)^2}}.$$

Now, as

$$\boldsymbol{\xi}^{\star}(\psi, s, t) = \check{\boldsymbol{r}}(\boldsymbol{\xi}(\psi, s, t), t) = \boldsymbol{\gamma}(s, t) + \epsilon(R(\psi, s, t)\cos\psi \, \boldsymbol{\eta}_1(s, t) + R(\psi, s, t)\sin\psi \, \boldsymbol{\eta}_2(s, t)),$$

is a parameterization of the lateral surface $\Gamma_{lat}^{\star}(t)$ in the spatial points, the mean curvature H of that surface is

$$H = -\frac{1}{2}\frac{(\boldsymbol{n}^{\star} \cdot \partial_{\psi\psi}\boldsymbol{\xi}^{\star})(\partial_s \boldsymbol{\xi}^{\star} \cdot \partial_s \boldsymbol{\xi}^{\star}) - 2(\boldsymbol{n}^{\star} \cdot \partial_{\psi s}\boldsymbol{\xi}^{\star})(\partial_\psi \boldsymbol{\xi}^{\star} \cdot \partial_s \boldsymbol{\xi}^{\star}) + (\boldsymbol{n}^{\star} \cdot \partial_{ss}\boldsymbol{\xi}^{\star})(\partial_\psi \boldsymbol{\xi}^{\star} \cdot \partial_\psi \boldsymbol{\xi}^{\star})}{(\partial_\psi \boldsymbol{\xi}^{\star} \cdot \partial_\psi \boldsymbol{\xi}^{\star})(\partial_s \boldsymbol{\xi}^{\star} \cdot \partial_s \boldsymbol{\xi}^{\star}) - (\partial_\psi \boldsymbol{\xi}^{\star} \cdot \partial_s \boldsymbol{\xi}^{\star})^2},$$

with outward-directed normal vector $\boldsymbol{n}^{\star}(\boldsymbol{\xi}^{\star}, t) = (\partial_\psi \boldsymbol{\xi}^{\star} \times \partial_s \boldsymbol{\xi}^{\star})/\|\partial_\psi \boldsymbol{\xi}^{\star} \times \partial_s \boldsymbol{\xi}^{\star}\|$ (see Do Carmo 1998). The resulting formula for H in terms of the radius function R and its derivatives is lengthy (see Marheineke & Wegener 2007, for details).

In addition to the geometrical quantities, the transformation of (2.2) requires the following characteristic quantities related to the coordinate transformation $\check{\boldsymbol{r}}$:

(*a*) Coordinate transformation matrix $\boldsymbol{F} = \nabla_{\boldsymbol{x}} \check{\boldsymbol{r}} = \boldsymbol{e}_i \otimes \boldsymbol{f}_i$,
with $\boldsymbol{f}_1 = \epsilon \, \boldsymbol{\eta}_1$, $\boldsymbol{f}_2 = \epsilon \, \boldsymbol{\eta}_2$, $\boldsymbol{f}_3 = (1 - \epsilon h)\, \boldsymbol{\tau}$

(*b*) Functional determinant $J = \det \boldsymbol{F} = \epsilon^2(1 - \epsilon h)$

(*c*) Inverse matrix $\boldsymbol{G} = \boldsymbol{F}^{-1} = \boldsymbol{g}_i \otimes \boldsymbol{e}_i$
with $\boldsymbol{g}_1 = \epsilon^{-1}\boldsymbol{\eta}_1$, $\boldsymbol{g}_2 = \epsilon^{-1}\boldsymbol{\eta}_2$, $\boldsymbol{g}_3 = (1 - \epsilon h)^{-1}\boldsymbol{\tau}$

(*d*) Coordinate velocity $\boldsymbol{q} = \partial_t \check{\boldsymbol{r}} = \partial_t \boldsymbol{\gamma} + \epsilon \, x_\alpha \partial_t \boldsymbol{\eta}_\alpha$

Because the time-dependent coordinate transformation $\check{\boldsymbol{r}}$ maps the scaled curvilinear coordinates $\boldsymbol{x}$ onto spatial points $\boldsymbol{r}$, we can consider any scalar, vector or tensor field in our problem relative to either spatial points or coordinates, i.e. $\tilde{f}(\boldsymbol{x}, t) = f(\check{\boldsymbol{r}}(\boldsymbol{x}, t), t)$. Here, we suppress the tilde that indicates this distinction to keep the notation simple. Moreover, in order to preserve the physical and geometrical meaning of the velocity and the stress in the subsequent curvilinear coordinate formulation of the free BVP

(2.7), we introduce the following special transformations for these quantities:

$$\boldsymbol{u} = (\boldsymbol{v} - \boldsymbol{q}) \cdot \boldsymbol{G}, \quad \boldsymbol{S} = J\, \boldsymbol{T} \cdot \boldsymbol{G}.$$

We refer to the above relation between the two velocities $\boldsymbol{u}$ and $\boldsymbol{v}$ as the coupling condition. The intrinsic velocity $\boldsymbol{u}$ describes the rate of convective transport of any observable in the coordinates, whereas the momentum-associated velocity $\boldsymbol{v}$ represents one of these transported quantities. Considering that $\boldsymbol{T}$ determines the forces on an arbitrary spatial surface, the second relation above ensures that $\boldsymbol{S}$ determines the same forces on the transformed surface in the curvilinear coordinates (see Antman 2006). Moreover, the functional determinant J represents a kind of density since the coordinate transformation $\check{\boldsymbol{r}}$ does not conserve volume.

In summary, we have now transformed the incompressible Navier–Stokes equations of the free BVP (2.2) in spatial coordinates into 'compressible' balance laws in the curvilinear coordinates, with a complex constitutive law and a distinction between transported and transporting velocity. The complete free BVP in the curvilinear coordinates is

$$\partial_t J + \nabla_{\boldsymbol{x}} \cdot (J\boldsymbol{u}) = 0, \tag{2.7a}$$

$$\partial_t (J\boldsymbol{v}) + \nabla_{\boldsymbol{x}} \cdot (\boldsymbol{u} \otimes J\boldsymbol{v}) = \nabla_{\boldsymbol{x}} \cdot \boldsymbol{S}^T + (J\boldsymbol{f}), \tag{2.7b}$$

$$\boldsymbol{u} = (\boldsymbol{v} - \boldsymbol{q}) \cdot \boldsymbol{G}, \tag{2.7c}$$

with the stress tensor

$$\begin{aligned}\boldsymbol{S} = &-p\,(\epsilon(1-\epsilon h)\,(\boldsymbol{\eta}_\alpha \otimes \boldsymbol{e}_\alpha) + \epsilon^2\,(\boldsymbol{\tau} \otimes \boldsymbol{e}_3)) \\ &+ \frac{1}{Re}\left(\epsilon(1-\epsilon h)(\partial_\alpha u_\beta + \partial_\beta u_\alpha)\,(\boldsymbol{\eta}_\alpha \otimes \boldsymbol{e}_\beta)\right. \\ &\quad + \left(\epsilon(1-\epsilon h)\partial_\alpha u_3 + \frac{\epsilon^3}{(1-\epsilon h)}\partial_s u_\alpha\right)(\boldsymbol{\eta}_\alpha \otimes \boldsymbol{e}_3) \\ &\quad + (\epsilon^2 \partial_s u_\alpha + (1-\epsilon h)^2 \partial_\alpha u_3)\,(\boldsymbol{\tau} \otimes \boldsymbol{e}_\alpha) \\ &\quad \left. + \left(2\epsilon^2 \partial_s u_3 + \frac{2\epsilon^3}{(1-\epsilon h)} h(\partial_\alpha u_\alpha + \partial_s u_3)\right)(\boldsymbol{\tau} \otimes \boldsymbol{e}_3)\right),\end{aligned} \tag{2.7d}$$

where $u_i := \boldsymbol{u} \cdot \boldsymbol{e}_i$, $i = 1, 2, 3$. The kinematic and dynamic boundary conditions for the lateral surface are

$$(\boldsymbol{u}(\boldsymbol{\xi}, t) - \partial_t \boldsymbol{\xi}) \cdot (\partial_\psi \boldsymbol{\xi} \times \partial_s \boldsymbol{\xi}) = 0, \quad \left(\boldsymbol{S} + \frac{\epsilon}{We} J H \boldsymbol{G}\right)(\boldsymbol{\xi}, t) \cdot (\partial_\psi \boldsymbol{\xi} \times \partial_s \boldsymbol{\xi}) = 0, \tag{2.7e}$$

and those for the bottom surface (in case of $|(\Gamma_{bot})(t)| > 0$) are

$$\frac{\mathrm{d}L}{\mathrm{d}t} = u_3, \quad \boldsymbol{S} \cdot \boldsymbol{e}_3 = 0. \tag{2.7f}$$

Together with the inflow profile $\boldsymbol{v} = \boldsymbol{v}_{in}$ and the initial condition $L(0) = 0$, the transformed free BVP is closed by the following constraints on the centreline:

$$\|\partial_s \boldsymbol{\gamma}\| = 1, \quad \boldsymbol{\gamma}(0, t) = \boldsymbol{\gamma}_0, \quad \partial_s \boldsymbol{\gamma}(0, t) = \boldsymbol{\tau}_0, \quad \int_{\mathscr{A}(s,t)} x_1 \,\mathrm{d}x_1 \,\mathrm{d}x_2 = \int_{\mathscr{A}(s,t)} x_2 \,\mathrm{d}x_1 \,\mathrm{d}x_2 = 0. \tag{2.7g}$$

The form of this BVP is derived in Panda *et al.* (2008) for homogeneous dynamic boundary conditions, i.e. assuming negligible surface tension. The above

inhomogeneous dynamic boundary conditions at the lateral surface result directly from the original spatial ones and the transformation of the stress $\boldsymbol{S} = J\boldsymbol{T}\cdot\boldsymbol{G}$. Concerning the bottom boundary, we must distinguish the two cases. If $|\Gamma_{bot}| = 0$, no further boundary conditions are necessary since the lateral surface equals the free surface up to a null set. On the other hand, if $|\Gamma_{bot}| > 0$, the bottom surface is planar in the coordinates and has the outward-directed normal vector $\boldsymbol{e}_3$ in accordance to our definition of the flow domain (2.4). Due to the linearity of the coordinate transformation in (x_1, x_2) (cf. (2.3)), the bottom surface in the spatial geometry inherits the planar shape and has thus zero mean curvature, i.e. $H = 0$. This leads to the boundary conditions stated above.

The unknowns of the transformed free BVP (2.7) are the field variables $\boldsymbol{v}$, p and the geometrical variables L, $\boldsymbol{\gamma}$, R. The intrinsic velocity $\boldsymbol{u}$ and the stress $\boldsymbol{S}$ are given by the coupling condition and the constitutive equation. All other quantities in the model ($\boldsymbol{\tau}$, $\boldsymbol{\eta}_1$, $\boldsymbol{\eta}_2$, h, $\boldsymbol{\xi}$, J, $\boldsymbol{G}$, H) are defined by the geometry.

2.2. *Cross-sectionally averaged balance laws*

The derivation of the one-dimensional asymptotic fibre model from the three-dimensional free BVP (2.7) is based on cross-sectional averaging of the balance laws. To formulate the averaging, we introduce the following notation for integrals over cross-sections and for line integrals over their boundary curves:

$$\langle f\rangle_{\mathscr{A}(s,t)} = \int_{\mathscr{A}(s,t)} f(x_1, x_2, s, t)\,\mathrm{d}x_1\,\mathrm{d}x_2, \quad \langle f\rangle_{\partial\mathscr{A}(s,t)} = \int_{\partial\mathscr{A}(s,t)} \frac{f}{\sqrt{n_1^2 + n_2^2}}\,\mathrm{d}l,$$

where f denotes a differentiable and integrable scalar- or vector-valued function on $\Omega(t)$ and $n_i := \boldsymbol{n}\cdot\boldsymbol{e}_i$, $i = 1, 2, 3$ are the components of the normal vector. By the Reynolds transport theorem, the relations

$$\langle \partial_s f\rangle_{\mathscr{A}(s,t)} = \partial_s\langle f\rangle_{\mathscr{A}(s,t)} + \langle f n_3\rangle_{\partial\mathscr{A}(s,t)}, \quad \langle \partial_t f\rangle_{\mathscr{A}(s,t)} = \partial_t\langle f\rangle_{\mathscr{A}(s,t)} - \langle f w\rangle_{\partial\mathscr{A}(s,t)}$$

hold (see Dewynne *et al.* 1992). Hence, the cross-sectionally averaged balance laws take the forms

$$\partial_t\langle J\rangle_{\mathscr{A}(s,t)} + \partial_s\langle J u_3\rangle_{\mathscr{A}(s,t)} = 0, \tag{2.8a}$$

$$\partial_t\langle J\boldsymbol{v}\rangle_{\mathscr{A}(s,t)} + \partial_s\langle J u_3\,\boldsymbol{v}\rangle_{\mathscr{A}(s,t)} = \partial_s\langle \boldsymbol{S}\cdot\boldsymbol{e}_3\rangle_{\mathscr{A}(s,t)} - \frac{\epsilon}{We}\langle JH\boldsymbol{G}\cdot\boldsymbol{n}\rangle_{\partial\mathscr{A}(s,t)} + \langle J\boldsymbol{f}\rangle_{\mathscr{A}(s,t)}. \tag{2.8b}$$

These equations are derived for the case $H = 0$ in Panda *et al.* (2008). The case $H \neq 0$ differs only in the expression for the averaged $\nabla_{\boldsymbol{x}}\cdot\boldsymbol{S}^T$, whose general form is

$$\langle \nabla_{\boldsymbol{x}}\cdot\boldsymbol{S}^T\rangle_{\mathscr{A}(s,t)} = \partial_s\langle \boldsymbol{S}\cdot\boldsymbol{e}_3\rangle_{\mathscr{A}(s,t)} + \langle \boldsymbol{S}\cdot\boldsymbol{n}\rangle_{\partial\mathscr{A}(s,t)}.$$

Substituting the inhomogeneous dynamic boundary conditions into the above expression we find that an additional term appears in the momentum law (2.8*b*) due to the fact that $\langle \boldsymbol{S}\cdot\boldsymbol{n}\rangle_{\partial\mathscr{A}(s,t)} = -\epsilon/We\langle JH\boldsymbol{G}\cdot\boldsymbol{n}\rangle_{\partial\mathscr{A}(s,t)}$. Using the parameterization $\boldsymbol{\xi}$ of $\Gamma_{lat}(t)$ and introducing the radius function R, we can express this line integral explicitly as

$$\langle JH\boldsymbol{G}\cdot\boldsymbol{n}\rangle_{\partial\mathscr{A}(s,t)} = \int_0^{2\pi} (\epsilon(1-\epsilon h)(\partial_\psi(R\sin\psi)\,\boldsymbol{\eta}_1 - \partial_\psi(R\cos\psi)\,\boldsymbol{\eta}_2) - \epsilon^2 R\partial_s R\,\boldsymbol{\tau})H\,\mathrm{d}\psi. \tag{2.9}$$

2.3. *Asymptotic analysis*

For the asymptotic analysis, the free BVP is embedded for a fixed slenderness parameter $\epsilon = \epsilon_0$ in a family of self-similar problems corresponding to parameters

$\epsilon \leqslant \epsilon_0$. For this family, we choose an ϵ-independent inflow domain in scaled curvilinear coordinates Γ_{in} as well as an ϵ-independent inflow velocity $\boldsymbol{v}_{in}$. This choice is enabled by the ϵ-independence of (2.6). All other quantities occurring in the BVP depend on ϵ, which we indicate by a subscript ϵ in the following. Their asymptotic expansions to zeroth- and first-order yield the cross-sectional properties required to evaluate the averaged balance laws of (2.8). For the field variables $\boldsymbol{v}$ and p and the geometrical quantities L, $\boldsymbol{\gamma}$ and R, we posit regular power series of the form

$$\boldsymbol{v}_\epsilon = \boldsymbol{v}^{(0)} + \epsilon \boldsymbol{v}^{(1)} + O(\epsilon^2),$$

from which the expansions of all other quantities in the problem can be derived. The local basis vectors $\boldsymbol{\tau}_\epsilon$, $\boldsymbol{\eta}_{1,\epsilon}$ and $\boldsymbol{\eta}_{2,\epsilon}$, the corresponding function h_ϵ and the parameterization of the lateral surface $\boldsymbol{\xi}_\epsilon$ are of zeroth order, while the functional determinant J_ϵ is of second order. Due to the decomposition of $\mathbf{G}_\epsilon = \boldsymbol{g}_{i,\epsilon} \otimes \boldsymbol{e}_i \sim O(\epsilon^{-1})$, the expansion of the intrinsic velocity has the form

$$\boldsymbol{u}_\epsilon = \epsilon^{-1} \boldsymbol{u}^{(-1)} + \boldsymbol{u}^{(0)} + \epsilon \boldsymbol{u}^{(1)} + O(\epsilon^2),$$

where in particular $u_3^{(-1)} = 0$ holds because $\boldsymbol{g}_{3,\epsilon} \sim O(1)$. The stress tensor $\mathbf{S}$ then turns out to be of zeroth order. Computing the mean curvature via the radius function gives

$$H_\epsilon = \epsilon^{-1} H^{(-1)} + H^{(0)} + \epsilon H^{(1)} + O(\epsilon^2),$$

thereby $2H^{(-1)}$ represents the zeroth-order curvature of the boundary curve $R^{(0)}$ in polar coordinates. The body force densities are assumed to be $\boldsymbol{f}_\epsilon \sim O(1)$ which stands in accordance to the gravitational and rotational forces we consider later in the application.

Note that we impose no restrictions on $\boldsymbol{\gamma}_\epsilon$, in contrast to Decent *et al.* (2002), Wallwork *et al.* (2002) and Decent *et al.* (2004) who assume a stationary centreline to leading order for their rotational spinning processes. But, since the shape tends to a circle under surface tension, we follow – in a weaker sense – their intuitive assumption of circular cross-sections by setting

$$R^{(0)} = R^{(0)}(s,t), \quad R^{(1)} = R^{(1)}(s,t). \tag{2.10}$$

This assumption enables the evaluation of the cross-sectionally averaged balance laws (2.8), which require knowledge of the relation between the fibre cross-sections and their boundary curves. But, it implies the restriction to a circular nozzle. Such assumptions about the shape were avoided by Cummings & Howell (1999), who showed that the evolution of the cross-sectional shape is generally governed by a quasi two-dimensional free boundary problem similar to two-dimensional Stokes flow with a surface tension-driven boundary and described by conformal mappings. However, since their approach assumes a nearly straight centreline, we cannot apply it to the curved centrelines of our rotational spinning process. With (2.10), the computation of the mean curvature to leading orders yields

$$H^{(-1)} = \frac{1}{2R^{(0)}}, \quad H^{(0)} = \frac{-R^{(0)} h^{(0)} - R^{(1)}}{2(R^{(0)})^2}. \tag{2.11}$$

Substituting these expansions into (2.7), the balance laws together with the dynamic lateral surface condition lead at zeroth and first order to two-dimensional Laplace problems and stress-free Stokes flows. The solution theory of these problems is based on the proof techniques of Dewynne *et al.* (1992) and formulated in Panda *et al.*

(2008) (Theorem 8, Corollaries 9 and 10): let a scalar-valued function φ as well as vector- and scalar-valued functions $\boldsymbol{\Phi}$ and f satisfy the general problems:

$$\begin{aligned} \triangle\varphi = 0, \quad \nabla\cdot\boldsymbol{\Phi} = c, \quad \triangle\boldsymbol{\Phi} = \nabla f, \quad &\text{in } \mathscr{D}, \\ \nabla\varphi\cdot\boldsymbol{n} = 0, \quad (\nabla\boldsymbol{\Phi} + \nabla\boldsymbol{\Phi}^T)\cdot\boldsymbol{n} = f\boldsymbol{n}, \quad &\text{on } \partial\mathscr{D}, \end{aligned}$$

on a bounded domain $\mathscr{D} \subset \mathbb{R}^2$ with outward-directed normal $\boldsymbol{n}$ and a given constant $c \in \mathbb{R}$. The solutions then have the form

$$\varphi(x_1, x_2) = d, \quad \boldsymbol{\Phi}(x_1, x_2) = \left(\frac{c}{2}x_1 - ax_2 + b_1, \frac{c}{2}x_2 + ax_1 + b_2\right), \quad f = c,$$

where a, b_1, b_2 and d are constant parameters. Applying this theory to our asymptotic problems, we identify $\mathscr{D}$ with the cross-sections $\mathscr{A}_0(s,t)$ given by $R^{(0)}(s,t)$ and embed all functions into $\mathscr{A}_0(s,t) \times [0, L^{(0)}(t))$. The parameters in our solution thus become functions of s and t. The restriction of the asymptotic analysis – even at first order – on the geometry at zeroth order is justified in Dewynne *et al.* (1992) and Cummings & Howell (1999) and formally proved in Panda *et al.* (2008) for our parameterization $\boldsymbol{\xi}_\epsilon$ using Taylor expansions of the boundary conditions. In the asymptotic problems at zeroth and first order, the general functions φ, $\boldsymbol{\Phi}$ and f have the specific identities:

$$\begin{aligned} &\varphi = u_3^{(0)}, \quad \boldsymbol{\Phi} = \left(u_1^{(-1)}, u_2^{(-1)}\right), \quad f = c = 0, \\ &\varphi = u_3^{(1)}, \quad \boldsymbol{\Phi} = \left(u_1^{(0)}, u_2^{(0)}\right), \quad f = Re\left(p^{(0)} - \frac{1}{We}H^{(-1)}\right), \ c = -\partial_s u_3^{(0)}. \end{aligned}$$

The satisfaction of the kinematic boundary conditions (2.7*e*) to leading orders requires the vanishing of the additive parameters $b_1(s,t)$ and $b_2(s,t)$ in both problems, but does not affect the choice of $a(s,t)$. At zeroth order, $a(s,t)$ would vanish for non-circular cross-sections. The degree of freedom in the considered circular case is gained from the coordinate transformation. However, the singularity that appears has no effect on our final result due to the centreline condition (2.5), as we will see below. At first order, $a(s,t)$ can be interpreted as twist (see Dewynne *et al.* 1994), but since it decouples from our final model we need not determine it. In addition, the satisfaction of the kinematic boundary conditions in (2.7*e*) associated to the first-order system leads also to the (cross-sectionally averaged) continuity equation for the asymptotic fibre model (2.12*a*). While this result is not surprising given that we require the boundary to be circular, it confirms the consistency of our assumption and the asymptotic analysis. Summing up, the intrinsic velocity and pressure profiles relevant for the further discussion are

$$\begin{gathered} u_1^{(-1)} = -a(s,t)x_2, \quad u_2^{(-1)} = a(s,t)x_1, \quad u_3^{(0)} = u_3^{(0)}(s,t), \\ p^{(0)} = -\frac{1}{Re}\partial_s u_3^{(0)}(s,t) + \frac{1}{We}H^{(-1)}(s,t), \end{gathered}$$

where the incorporation of surface tension modifies the pressure in comparison to Panda *et al.* (2008). Moreover, the asymptotic analysis yields the following expressions for the momentum-associated velocity and the stresses:

$$\boldsymbol{v}^{(0)} = u_\alpha^{(-1)}\boldsymbol{\eta}_\alpha^{(0)} + u_3^{(0)}\boldsymbol{\tau}^{(0)} + \partial_t\boldsymbol{\gamma}^{(0)}, \quad \boldsymbol{S}^{(0)} = \boldsymbol{S}^{(1)} = 0.$$

The cross-sectionally averaged balance laws (2.8) provide the closure for the asymptotic analysis. Considering (2.8*b*) and noting that $\boldsymbol{S}^{(0)}$ and $\boldsymbol{S}^{(1)}$ vanish, we see that only the axial effect of the second-order stress is of interest. With the asymptotic

results of zeroth and first order, its explicit form is

$$\boldsymbol{S}^{(2)}\cdot\boldsymbol{e}_3 = -p^{(0)}\boldsymbol{\tau}^{(0)} + \frac{1}{Re}\big(2\big(\partial_s u_3^{(0)} - u_\alpha^{(-1)}\partial_\alpha h\big)\boldsymbol{\tau}^{(0)} + \partial_s u_\alpha^{(-1)}\boldsymbol{\eta}_\alpha^{(0)}\big).$$

Using this together with the centreline condition (2.5) and the expression for $p^{(0)}$, we obtain

$$\langle \boldsymbol{S}^{(2)}\cdot\boldsymbol{e}_3\rangle_{\mathscr{A}_0} = \left(\frac{3}{Re}|\mathscr{A}_0|\,\partial_s u_3^{(0)} - \frac{\sqrt{\pi}}{2We}\sqrt{|\mathscr{A}_0|}\right)\boldsymbol{\tau}^{(0)}.$$

The line integral over the boundary in (2.8*b*)/(2.9) vanishes consistently at zeroth order because of (2.11). At first order, it is explicitly given by

$$(\langle JH\boldsymbol{G}\cdot\boldsymbol{n}\rangle_{\partial\mathscr{A}})^{(1)} = -\sqrt{\pi}\,\partial_s\big(\sqrt{|\mathscr{A}_0|}\,\boldsymbol{\tau}^{(0)}\big).$$

Consequently, the averaged balance laws at their leading order yield the following asymptotic fibre model:

$$\partial_t|\mathscr{A}_0| + \partial_s\big(u_3^{(0)}|\mathscr{A}_0|\big) = 0, \tag{2.12a}$$

$$\partial_t(\langle\boldsymbol{v}^{(0)}\rangle_{\mathscr{A}_0}) + \partial_s\big(u_3^{(0)}\langle\boldsymbol{v}^{(0)}\rangle_{\mathscr{A}_0}\big) = \partial_s\left(\left(\frac{3}{Re}|\mathscr{A}_0|\,\partial_s u_3^{(0)} + \frac{\sqrt{\pi}}{2We}\sqrt{|\mathscr{A}_0|}\right)\boldsymbol{\tau}^{(0)}\right) + \langle\boldsymbol{f}^{(0)}\rangle_{\mathscr{A}_0}, \tag{2.12b}$$

together with the coupling and geometrical conditions (cf. page 355 for the respective expansions)

$$\langle\boldsymbol{v}^{(0)}\rangle_{\mathscr{A}_0} = \big(u_3^{(0)}(s,t)\boldsymbol{\tau}^{(0)}(s,t) + \partial_t\boldsymbol{\gamma}^{(0)}(s,t)\big)\,|\mathscr{A}_0|, \tag{2.12c}$$

$$\big\|\partial_s\boldsymbol{\gamma}^{(0)}\big\| = 1. \tag{2.12d}$$

In the momentum equation, only the cross-sectionally averaged velocity, and not the exact profile, is of interest. Its exclusive dependence on the tangential intrinsic velocity and the dynamics of the centreline is deduced from the centreline condition.

2.4. *Initial and boundary conditions*

Closing the one-dimensional fibre model (2.12) requires appropriate leading-order initial and boundary conditions. As $\Omega(0)=\emptyset$, the initial condition is $L^{(0)}(0)=0$, and the initial bottom surface is formally prescribed by the nozzle area. Obviously, the asymptotic theory is not valid for the initial stage of the process because the fibre is not slender. Nevertheless, lacking a better initialization, we use the model even for this stage. The ϵ independence of the inflow domain implies the following boundary conditions at the nozzle:

$$\boldsymbol{\gamma}^{(0)}(0,t) = \boldsymbol{\gamma}_0, \quad \partial_s\boldsymbol{\gamma}^{(0)}(0,t) = \boldsymbol{\tau}_0, \quad |\mathscr{A}_0|(0,t) = 1,$$

together with

$$u_3^{(0)}(0,t) = 1,$$

which is a consequence of $\langle\boldsymbol{v}_{in}\rangle_{\mathscr{A}_0(0,t)} = \langle\boldsymbol{v}^{(0)}\rangle_{\mathscr{A}_0(0,t)} = u_3^{(0)}(0,t)\boldsymbol{\tau}_0$.

It remains to deduce the kinematic and dynamic boundary conditions for the free end of the fibre. For the case $|\Gamma_{bot}|>0$, these conditions are just the averaged leading-order contributions to (2.7*f*). However, in the presence of surface tension, it seems physically more realistic to suppose that the end shrinks to a single point. The analytical continuation of the lateral boundary conditions to such an end point, which would be the logical approach, fails in the asymptotics due to the

breakdown of the slender body assumptions (see also Eggers & Dupont 2001). We overcome this problem using a volume-averaging approach that is successful in both cases, i.e. $|\Gamma_{bot}| \geqslant 0$. In particular, we deduce the missing boundary conditions by comparing the volume-averaged three-dimensional and the line-averaged one-dimensional balance laws at leading order.

Integrating (2.8) over the arclength parameter s yields the volume-averaged three-dimensional balance laws

$$\frac{\mathrm{d}}{\mathrm{d}t}\int_0^{L_\epsilon(t)} \langle J_\epsilon \rangle_{\mathscr{A}_\epsilon(s,t)}\,\mathrm{d}s - \langle J_\epsilon \boldsymbol{u}_\epsilon \cdot \boldsymbol{e}_3\rangle_{\mathscr{A}_\epsilon(0,t)} = 0,$$

$$\frac{\mathrm{d}}{\mathrm{d}t}\int_0^{L_\epsilon(t)} \langle J_\epsilon \boldsymbol{v}_\epsilon \rangle_{\mathscr{A}_\epsilon(s,t)}\,\mathrm{d}s - \langle J_\epsilon \boldsymbol{v}_\epsilon \boldsymbol{u}_\epsilon \cdot \boldsymbol{e}_3\rangle_{\mathscr{A}_\epsilon(0,t)}$$

$$= -\langle \boldsymbol{S}_\epsilon \cdot \boldsymbol{e}_3\rangle_{\mathscr{A}_\epsilon(0,t)} - \frac{\epsilon}{We}\int_0^{L_\epsilon(t)} \langle J_\epsilon H_\epsilon \boldsymbol{G}_\epsilon \cdot \boldsymbol{n}_\epsilon\rangle_{\partial\mathscr{A}_\epsilon(s,t)}\,\mathrm{d}s + \int_0^{L_\epsilon(t)} \langle J_\epsilon \boldsymbol{f}_\epsilon\rangle_{\mathscr{A}_\epsilon(s,t)}\,\mathrm{d}s.$$

The left-hand sides in the above expressions are obtained using the averaging techniques described in § 2.2 together with the kinematic boundary conditions. The integral over the bottom surface $\langle \boldsymbol{S}_\epsilon \cdot \boldsymbol{e}_3\rangle_{\mathscr{A}_\epsilon(L(t),t)}$ on the right-hand side of the momentum equation vanishes since either $|\mathscr{A}_\epsilon(L_\epsilon(t),t)| = 0$ for a single fibre end point or $H_\epsilon = 0$ for a planar bottom surface (cf. dynamic boundary conditions in (2.7f)). Consequently, we get to leading order

$$\int_0^{L^{(0)}(t)} \partial_t|\mathscr{A}_0|\,\mathrm{d}s + \frac{\mathrm{d}L^{(0)}(t)}{\mathrm{d}t}|\mathscr{A}_0|\big(L^{(0)}(t),t\big) - \big(u_3^{(0)}|\mathscr{A}_0|\big)(0,t) = 0,$$

$$\int_0^{L^{(0)}(t)} \partial_t\langle \boldsymbol{v}^{(0)}\rangle_{\mathscr{A}_0(s,t)}\,\mathrm{d}s + \frac{\mathrm{d}L^{(0)}(t)}{\mathrm{d}t}\big\langle \boldsymbol{v}^{(0)}\big\rangle_{\mathscr{A}_0(L^{(0)}(t),t)} - u_3^{(0)}(0,t)\big\langle \boldsymbol{v}^{(0)}\big\rangle_{\mathscr{A}_0(0,t)}$$

$$= \frac{\sqrt{\pi}}{We}\big(\sqrt{|\mathscr{A}_0|}\boldsymbol{\tau}^{(0)}\big)\big(L^{(0)}(t),t\big) - \left(\left(\frac{3}{Re}|\mathscr{A}_0|\,\partial_s u_3^{(0)} + \frac{\sqrt{\pi}}{2We}\sqrt{|\mathscr{A}_0|}\right)\boldsymbol{\tau}^{(0)}\right)(0,t)$$

$$+ \int_0^{L^{(0)}(t)} \big\langle \boldsymbol{f}^{(0)}\big\rangle_{\mathscr{A}_0(s,t)}\,\mathrm{d}s.$$

Integrating the one-dimensional fibre equations (2.12) over $s \in [0, L^{(0)}(t))$ leads to a similar but slightly different set of equations. Requiring the difference between the two to be zero yields the desired kinematic and dynamic boundary conditions, i.e.

$$\frac{\mathrm{d}L^{(0)}(t)}{\mathrm{d}t} = u_3^{(0)}\big(L^{(0)}(t),t\big), \quad \big(|\mathscr{A}_0|\,\partial_s u_3^{(0)}\big)\big(L^{(0)}(t),t\big) = \frac{\sqrt{\pi}}{6}\frac{Re}{We}\sqrt{|A_0|}\big(L^{(0)}(t),t\big). \quad (2.13)$$

Setting $u = u_3^{(0)}$, $\boldsymbol{v} = \langle \boldsymbol{v}^{(0)}\rangle_{\mathscr{A}_0}/|\mathscr{A}_0|$, $\boldsymbol{f} = \langle \boldsymbol{f}^{(0)}\rangle_{\mathscr{A}_0}/|\mathscr{A}_0|$ and $A = |\mathscr{A}_0|$ and dropping the superscripts $^{(0)}$ in (2.12) and (2.13), we obtain the one-dimensional model (1.1) describing the fibre dynamics.

3. Numerical results and discussion

The asymptotic model derived above describes the spinning of a slender curved inertial viscous Newtonian fibre with surface tension. It determines the dynamics of the fibre centreline $\boldsymbol{\gamma}$, the cross-sectional area A, the intrinsic velocity u and the momentum-associated velocity $\boldsymbol{v}$, as well as the temporal evolution of the fibre length L. Our balance laws for mass and momentum place no restrictions on the motion or shape of the fibre centreline, and account for both the inner viscous transport

and surface tension. Our model thus includes most of those previously developed for nearly straight and curved centrelines, as we will show in more detail below. Extending particularly the work on curved fibres by Decent *et al.* (2002), Wallwork *et al.* (2002), Decent *et al.* (2004) and Panda *et al.* (2008) to non-stationary centrelines with surface tension, our model can be regarded as a generalized theory of viscous 'strings'. The decoupling of the angular momentum effects that are characteristic for a 'rod' theory results from our choice of the non-stationary geometrical centreline as reference curve. The viscous 'rod' approach by Ribe (2004) and Ribe *et al.* (2006*a*) is based on a material curve in a scenario without surface tension. Both approaches coincide for negligibly small transversal forces in a stationary case, since then Ribe's complex system of linear and angular momentum equations decomposes.

In our model, the axial stress

$$\boldsymbol{s}_{tot} = \boldsymbol{s}_{vis} + \boldsymbol{s}_{surf} = \left(\frac{3}{Re} A \partial_s u + \frac{\sqrt{\pi}}{2We} \sqrt{A} \right) \partial_s \boldsymbol{\gamma},$$

includes contributions from both viscosity and surface tension. The first term represents the Trouton viscosity (see Trouton 1906), while the second term is the leading-order contribution of the mean curvature. By rewriting the dynamic boundary condition as $\boldsymbol{s}_{vis}(L(t), t) = \boldsymbol{s}_{surf}(L(t), t)$, we see that the viscous stresses balance the surface tension at the fibre end. Our model predicts asymptotically a finite cross-sectional area $A(L(t), t)$ whose temporal evolution depends on the ratio of viscous forces and surface tension measured by the capillary number $Ca = We/Re$. At first glance, this seems to involve a contradiction: no surface tension acts on a planar bottom surface, nor is a planar bottom surface physically realistic in the presence of surface tension. However, note that we never assumed the end to be planar for $t > 0$ in the description of the three-dimensional problem. Rather, model (2.7) enables the treatment of both possibilities, a single end point as well as a bottom surface. However, our asymptotic model (1.1) predicts a finite bottom surface at leading order such that the apparent contradiction occurs between the physical perception of the spatial ending and the asymptotic result. This observation suggests the existence of a boundary layer of length ϵ in the three-dimensional BVP that is not described by (1.1). Nevertheless, its effect on the fibre dynamics should be localized, because our balance laws come from a systematic derivation and the boundary conditions from a global balance. To incorporate the layer in the one-dimensional theory, it might be useful to extend the asymptotics to higher order, including axial curvature (see Eggers 1997, for uniaxial flow). Such a theory should be able to describe more effects arising from surface tension. As a destabilizing mechanism to the flow, it drives instabilities that lead to fibre breakup and drop formation (Eggers & Dupont 2001; Sierou & Lister 2003; Wong *et al.* 2004; Partridge *et al.* 2005).

A simple differential equation that describes the evolution of the area at the fibre end can be obtained by combining conservation of mass and the boundary conditions, and is

$$\frac{\mathrm{d}A(L(t), t)}{\mathrm{d}t} = -(A \partial_s u)(L(t), t) = -\frac{\sqrt{\pi}}{6Ca} \sqrt{A}(L(t), t), \quad A(0, 0) = 1.$$

Its unique solution is

$$A(L(t), t) = \begin{cases} (1 - t/t_c)^2, & t \leqslant t_c \\ 0, & t > t_c \end{cases}, \quad t_c = \frac{12}{\sqrt{\pi}} Ca, \tag{3.1}$$

since $A \geqslant 0$. Note that our model ceases to be valid when $A(L(t), t) = 0$ due to the definition of the fibre domain (2.4). Accordingly, the numerical simulations described below are performed for $t < t_c$.

The evolution of the end surface of the fibre is independent of the body forces whose specification closes the underlying free BVP. In the application to rotational spinning the force densities $\boldsymbol{f}$ are due to gravity and rotation,

$$\boldsymbol{f} = \frac{1}{Fr^2}\,\boldsymbol{e_g} - \frac{2}{Rb}\,(\boldsymbol{e_\omega} \times \boldsymbol{v}) - \frac{1}{Rb^2}\,(\boldsymbol{e_\omega} \times (\boldsymbol{e_\omega} \times \boldsymbol{\gamma})),$$

where $g\,\boldsymbol{e_g} = \boldsymbol{g}$ is the acceleration of gravity and $\omega\,\boldsymbol{e_\omega} = \boldsymbol{\omega}$ the angular velocity of the rotating device with radius ℓ. The rotation axis goes through the origin. The dimensionless Froude number $Fr = V/\sqrt{g\ell}$ and Rossby number $Rb = V/(\omega\ell)$ characterize the relation between inertial and gravitational forces and between inertial and rotational forces, respectively.

To study the effects of surface tension, viscosity, gravity and rotation on the fibre dynamics, we perform numerical simulations for different values of the characteristic dimensionless groups (*We*, *Re*, *Fr* and *Rb*). We begin with the special case of uniaxial flow under gravity, for which the asymptotic model takes a particularly simple form while still retaining the characteristic behaviour (3.1) of the free end, and proceed thence to more general cases of fibres with curved centrelines. In devising a numerical scheme, it is important to suppress surface tension-driven instabilities, modes with arbitrarily short wavelength and finite growth rate, of the kind analysed in Eggers (1997) and Eggers & Dupont (2001) for uniaxial flows. One way to do this is to abandon the formal asymptotic analysis on physical grounds by replacing the leading-order mean curvature by the full expression for the mean curvature of a jet with circular cross-sections and straight centreline. This approach can be rigorously justified for a uniaxial flow, but has also been successfully applied to curved flows (Entov & Yarin 1984; Yarin 1993; Eggers & Dupont 2001; Wallwork *et al.* 2002). Instead of such a regularization with axial curvature, we choose to damp the instabilities numerically in this paper. The essence of our algorithm is a finite-volume method on a staggered grid with implicit upwind flux discretization, with a new cell added at each time step to account for the increasing length of the fibre. More details of the implementation are given in Panda (2006).

3.1. *Uniaxial flow under gravity*

The special case of uniaxial flow arises when a spatially fixed spinning nozzle injects the fibre vertically downward, in the direction of gravity $\boldsymbol{e_g}$. This situation can be described by setting $\boldsymbol{\tau}_0 = \boldsymbol{e_g}$ and $\mathrm{Rb} \to \infty$ in (1.1), whereupon our model equations reduce to a system for A, u and L :

$$\partial_t A + \partial_s(uA) = 0,$$
$$\partial_t(Au) + \partial_s(u^2 A) = \partial_s\left(\frac{3}{Re} A\partial_s u + \frac{\sqrt{\pi}}{2We}\sqrt{A}\right) + \frac{1}{Fr^2}A,$$

together with the boundary conditions $A(0, t) = 1$, $u(0, t) = 1$ at the nozzle and

$$\frac{\mathrm{d}L(t)}{\mathrm{d}t} = u(L(t), t), \quad L(0) = 0 \quad (A\partial_s u)(L(t), t) = \frac{\sqrt{\pi}}{6}\frac{Re}{We}\sqrt{A}(L(t), t),$$

at the free end. Because the geometrical constraint is satisfied identically, the centreline variable $\boldsymbol{\gamma}$ does not enter the problem. Moreover, the momentum equation becomes scalar-valued, since the coupling condition reduces to $\boldsymbol{v} = u\,\boldsymbol{e_g}$ and the force densities to

$\boldsymbol{f} = \boldsymbol{e}_g/Fr^2$. In spite of the simplifications, the essential characteristics of the temporal evolution of the free end described by (3.1) are retained.

The unidirectional balance laws are well known in the context of glass fibre drawing, where a fibre of fixed length is stretched by a pulling velocity applied to its end (see, e.g. Pearson & Matovich 1969; Pearson 1985; Caroselli 1999), and the stability of these equations has been analysed (see, e.g. Geyling & Homsey 1980; Gospodinov & Roussinov 1993; Eggers 1997; Yarin *et al.* 1999). For the case of a free end without surface tension, numerical schemes are presented, e.g. in Stokes *et al.* (2000), Stokes & Tuck (2004) and Panda (2006). Stokes & Tuck (2004) used a finite element method in terms of a Lagrangian framework to simulate the extensional fall of viscous drops, whereas Panda (2006) developed a numerical scheme based on a finite-volume method on a staggered grid in Eulerian coordinates. Here we extend the latter approach incorporating the dynamic boundary conditions associated with surface tension. Our numerical results coincide with those in Stokes & Tuck (2004) and Panda (2006) for $We \to \infty$, in which case the bottom cross-section preserves the initial area $A(L(t), t) = A(0, 0)$ because $\partial_s u(L(t), t) = 0$. This effect is confined to a boundary layer and has almost no influence on the behaviour of the rest of the fibre, see Yarin (1993) and figure 3 for $We = 10$.

Figures 3 and 4 illustrate the temporal evolution of the fibre properties, i.e. cross-section A, velocity u and stresses s_{tot}, s_{vis}, s_{surf} over the arclength s, for three different scenarios with varying Weber number $We \in \{0.25, 1, 10\}$ and fixed Froude and Reynolds numbers $(Fr, Re) = (0.5, 1)$. Thereby, the scaling of the axes is not chosen equally but adapted to the focus of interest. Considering the free fibre end, the numerical simulations confirm the force balance between viscous and surface tension ($\mathrm{s}_{vis}(L(t), t) = \mathrm{s}_{surf}(L(t), t)$), and moreover reproduce quantitatively the theoretical prediction of $A(L(t), t)$. The lower the Weber number, i.e. the larger the surface tension, the faster is the decrease of the cross-section at the free end. The scalar-valued tension s_{tot} in the fibre is dominated by the contribution of surface tension $\mathrm{s}_{surf} = \sqrt{\pi A}/(2We)$, whereas the viscous tension $\mathrm{s}_{vis} = 3A\partial_s u/Re$ decays rapidly to zero (see figure 4). When the viscous stresses become negative because of a sign change of $\partial_s u$, our numerical simulations break down due to non-convergence of our implicit solver. The higher the Weber number, the longer it takes to reach this point, as also observed in Wallwork *et al.* (2002), Wong *et al.* (2004) and Partridge *et al.* (2005). However, we expect our model to be valid up to the time of breakup where $A = 0$, according to detailed investigations of the model equations with a prescribed end and their extension including axial curvature (Eggers 1997; Eggers & Dupont 2001).

3.2. *Curved flow under gravitation and rotation*

For the simulation of rotational spinning (figure 1), we use the full model (1.1). In particular, we consider a situation in which a fibre is ejected horizontally from a spinning nozzle located on the curved face of a cylindrical drum with unit dimensionless radius that rotates about its vertical symmetry axis. Symbolically, this implies $\boldsymbol{e}_{\boldsymbol{\omega}} = -\boldsymbol{e}_g = \boldsymbol{e}_3$ and $\boldsymbol{\gamma}_0 = \boldsymbol{\tau}_0 = \boldsymbol{e}_1$ where $\boldsymbol{e}_1$, $\boldsymbol{e}_2$ and $\boldsymbol{e}_3$ denote the canonical basis of $\mathbb{R}^3$ in the rotating reference frame. Figures 5–7 show the temporal evolution of the cross-section A, the intrinsic velocity u and the projection of the fibre centreline onto the $\boldsymbol{e}_1$–$\boldsymbol{e}_2$-plane, for different combinations of values of the dimensionless parameters. Our results for high Reynolds number (small viscosity) agree well with those of Wallwork *et al.* (2002), Decent *et al.* (2004) and Wong *et al.* (2004): the smaller the Rossby number, i.e. the faster the rotation, the more pronounced is the curling of the fibre in the $\boldsymbol{e}_1$–$\boldsymbol{e}_2$-plane. The curling is also influenced by the surface tension.

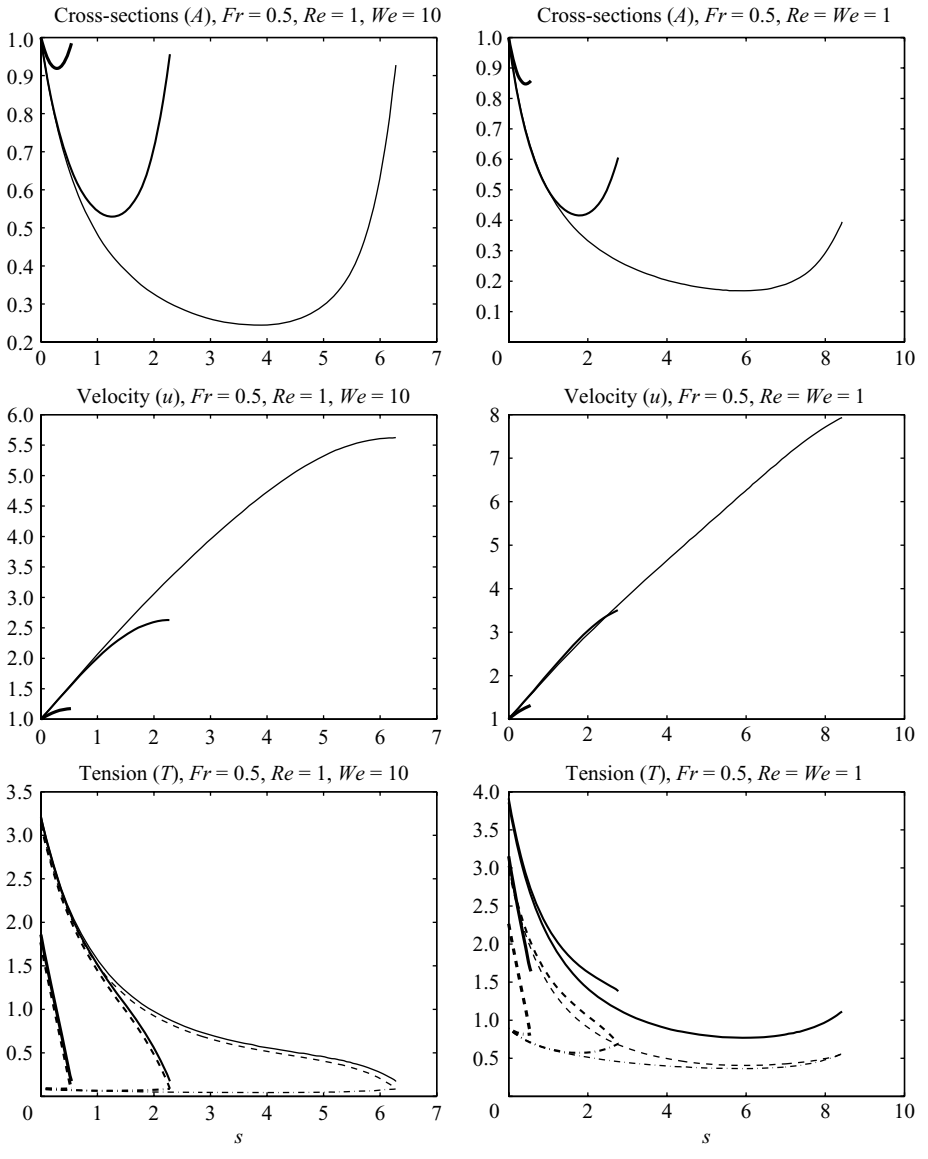

FIGURE 3. Uniaxial flow. Top to bottom: temporal evolution of A, u and stresses s_{tot} (–), s_{vis} (- -), s_{surf} (-.) for $t \in \{0.5, 1.5, 2.5\}$, $Fr = 0.5$, $Re = 1$. Left, $We = 10$ with $t_c = 67.7$. Right, $We = 1$ with $t_c = 6.7$. Note that the scaling of the axes is different for the three cases.

Moreover, decreasing the Weber number, i.e. increasing the surface tension, accelerates the thinning of the end of the fibre as in the case of uniaxial flow. The critical time $t_c = 12We/(\sqrt{\pi}Re)$ when the end of the fibre shrinks to a point is observed in the simulations. In contrast to the approach of Wallwork *et al.* (2002) and Decent *et al.* (2004) which is restricted to a stationary centreline, our model allows the numerical simulation of a non-stationary fibre centreline, which is important for fast rotation and small Reynolds number flow, as illustrated in figures 6 and 1 (see also Panda *et al.* 2008, for visualizations of this effect). An important manifestation of non-stationarity in rotational glass spinning processes is the recoil of a highly

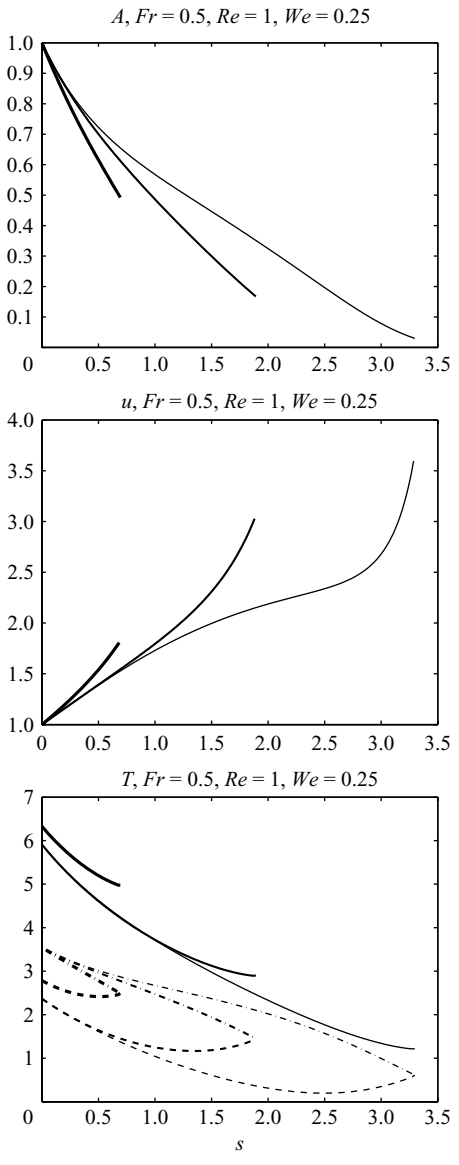

FIGURE 4. Uniaxial flow. Top to bottom: temporal evolution of A, u and stresses s_{tot} (–), s_{vis} (- -), s_{surf} (-.) for $t \in \{0.5, 1, 1.5\}$, $Fr = 0.5$, $Re = 1$, $We = 0.25$ with $t_c = 1.7$.

viscous fibre after drop detachment; see the 'dynamic breakup mode 4' observed by Wong *et al.* (2004).

Note, however, that the applicability of our model is restricted to certain parameter ranges. Physically relevant solutions for the model for stationary flow without surface tension exist only for $Re^{-1} < Rb^2$, $Rb \to 0$, $Re \to \infty$ (for the proof see Götz *et al.* 2008). When surface tension is included, the question of existence is more difficult to answer and left to future research. Moreover, for small Weber numbers (high surface tension), we encounter numerical problems at the nozzle, because the fluid exits at an angle different than the nominal (perpendicular) exit angle. The boundary layer that results seems to cause a failure of the slender body theory, which, however, might

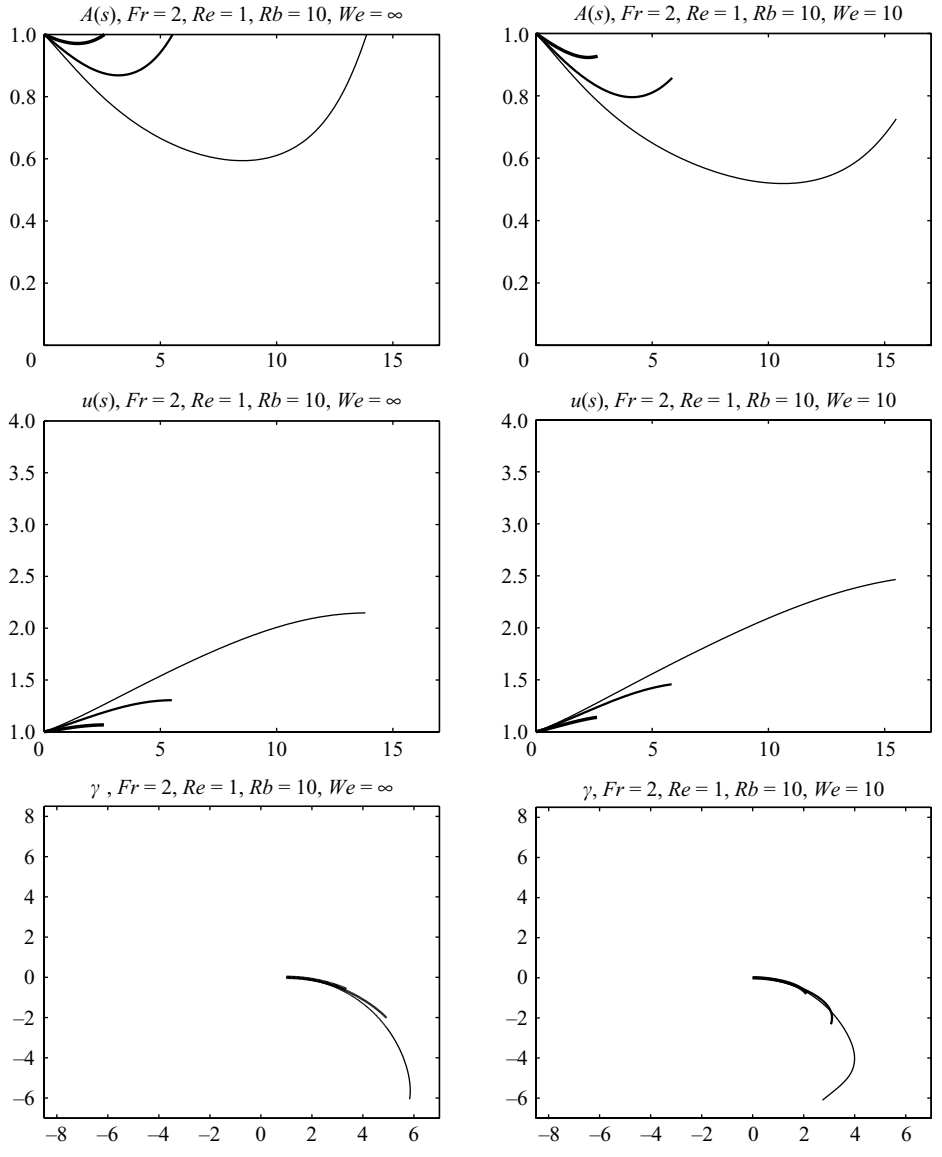

FIGURE 5. Curved flow. Top to bottom: temporal evolution of A, u and the projection of $\boldsymbol{\gamma}$ onto the $\boldsymbol{e}_1$–$\boldsymbol{e}_2$-plane (i.e. top view), for $t \in \{2.5, 5, 10\}$, $Fr = 2$, $Re = 1$, $Rb = 10$. Left, $We = \infty$. Right, $We = 10$.

be overcome by using modified boundary conditions at the nozzle. This remains to be further investigated (see also Finnicum *et al.* 1993; Eggers & Dupont 2001; Decent *et al.* 2002; Wallwork *et al.* 2002 on this point). Alternatively, the analysis of the angular momentum effects and the remaining ϵ-dependence in the model of Ribe *et al.* (2006*a*) raises hope that a generalized non-stationary 'rod' theory might handle these problems, in analogy to the previous studies on 'string' and 'rod' models for fluid-mechanical sewing machines by Chiu-Webster & Lister (2006) and Ribe, Lister & Chiu-Webster (2006*b*).

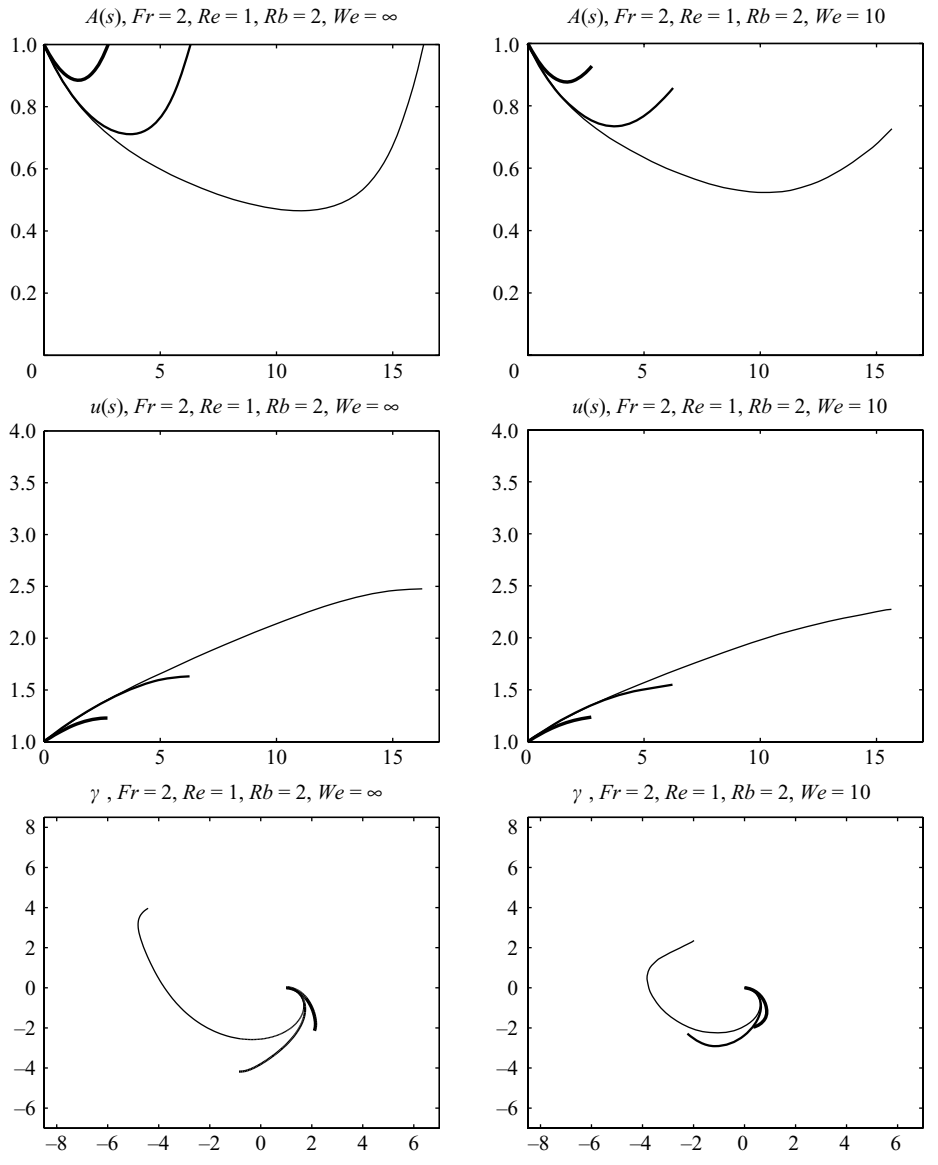

FIGURE 6. Curved flow. Top to bottom: temporal evolution of A, u and of the projection of $\boldsymbol{\gamma}$ in $\boldsymbol{e}_1$–$\boldsymbol{e}_2$-plane (i.e. top view), for $t \in \{2.5, 5, 10\}$, $Fr = 2$, $Re = 1$, $Rb = 2$. Left, $We = \infty$. Right, $We = 10$.

4. Conclusion

The asymptotic one-dimensional model for fibre dynamics that we have derived in this paper allows the simulation of non-stationary curved highly viscous fibres with surface tension and free ends as they occur in rotational spinning processes. Our balance laws for mass and momentum, which generalize those used in several previous studies, place no restrictions on the motion or shape of the fibre centreline and account fully for both inner viscous transport and surface tension. The boundary conditions we have deduced for the free end give quantitative information about its temporal evolution as a function of the ratio of viscous forces and surface tension. A deeper

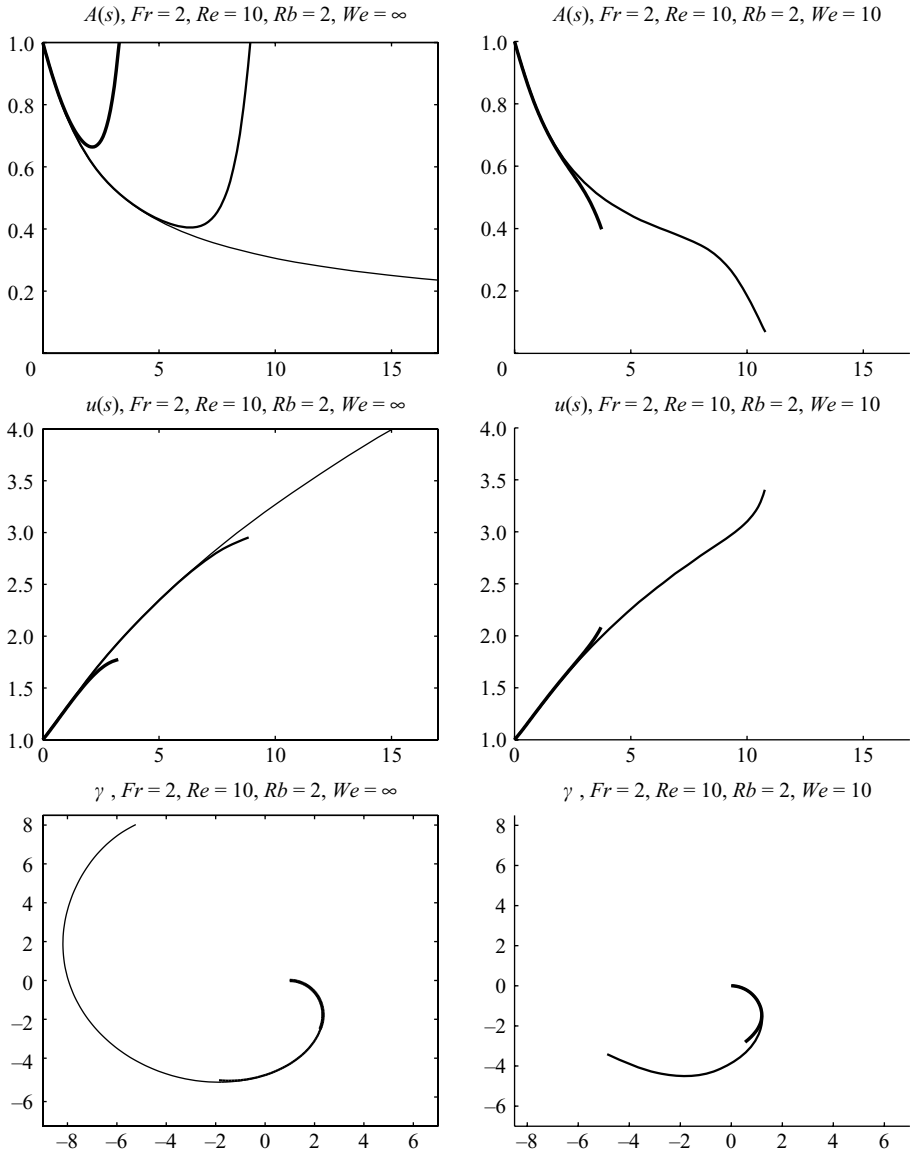

FIGURE 7. Curved flow. Top to bottom: temporal evolution of A, u and of the projection of $\boldsymbol{\gamma}$ in $\boldsymbol{e}_1$–$\boldsymbol{e}_2$-plane (i.e. top view), $Fr = 2$, $Re = 10$, $Rb = 2$. Left, $We = \infty$ for $t \in \{2.5, 5, 10\}$. Right, $We = 10$ for $t \in \{2.5, 5\}$; note that $t_c = 6.8$.

insight into the effects at the fibre end might be obtained by including axial curvature in the model. Numerical simulations performed using the model are physically realistic, except when $Re^{-1} > Rb^2$ or when the Weber number is very small. The failure takes the form of unphysical behaviour near the nozzle indicating that the slender body theory breaks down due to the presence of a transition region or boundary layer there. The problem might be overcome by imposing modified boundary conditions on the nozzle exit angle, but this requires further theoretical and numerical investigation. Future extensions of the model with a view towards practical applications include the incorporation of aerodynamic forces and temperature dependence.

This work has been supported by the Rheinland-Pfalz Excellence Center for Mathematical and Computational Modeling $(CM)^2$. Moreover, we would like to acknowledge the three anonymous referees for valuable hints and suggestions. Our special thanks go to our colleague Neil M. Ribe for proofreading the manuscript and giving helpful comments.

Appendix

The appendix is meant to facilitate the comparability of our asymptotic model to those in literature. In particular, the meaning of our intrinsic velocity u and its derivative $\partial_s u$ is discussed in more detail.

Mathematically, u acts as Lagrangian parameter to the arclength constraint $\|\partial_s \boldsymbol{\gamma}\| = 1$ in our model equations (1.1*a*)–(1.1*c*) for cross-section A, linear momentum $A\boldsymbol{v}$ and centreline $\boldsymbol{\gamma}$. To understand the physical meaning of u, we introduce a transformation ψ by the following differential equation:

$$\partial_t \psi(\sigma, t) = u(\psi(\sigma, t), t) \quad \text{equipped with appropriate initial condition,} \tag{A 1}$$

and re-parametrize centreline and momentum-associated velocity according to

$$\hat{\boldsymbol{\gamma}}(\sigma, t) = \boldsymbol{\gamma}(\psi(\sigma, t), t), \quad \hat{\boldsymbol{v}}(\sigma, t) = \boldsymbol{v}(\psi(\sigma, t), t). \tag{A 2}$$

In the new parametrization, the coupling condition (1.1*c*) becomes $\partial_t \hat{\boldsymbol{\gamma}} = \hat{\boldsymbol{v}}$, indicating a material description. This means that $\psi(\sigma, t)$ is the arclength parameter associated to the material point σ on the fibre and u is the temporal rate of its change (cf. (A 1)).

Differentiating (A 1) and (A 2) with respect to σ, we obtain

$$\partial_s u(\psi(\sigma, t), t) = \frac{\partial_t \|\partial_\sigma \hat{\boldsymbol{\gamma}}\|}{\|\partial_\sigma \hat{\boldsymbol{\gamma}}\|}(\sigma, t),$$

with the help of the arclength constraint. Consequently, $\partial_s u$ represents the relative rate of stretching that can also be related to the curvature κ of the centreline and the tangential and normal components of the momentum-associated velocity

$$\partial_s u = \partial_s v_\tau - \kappa v_\eta, \tag{A 3}$$

with $v_\tau = \boldsymbol{v} \cdot \boldsymbol{\tau}$, $v_\eta = \boldsymbol{v} \cdot \boldsymbol{\eta}$, $\boldsymbol{\tau} = \partial_s \boldsymbol{\gamma}$, $\boldsymbol{\eta} = \partial_{ss} \boldsymbol{\gamma}/\kappa$ and $\kappa = \|\partial_{ss} \boldsymbol{\gamma}\|$. The above relation results from projecting our coupling condition (1.1*c*) in tangential direction and differentiating it with respect to the arclength parameter. Relation (A 3) plays an essential role in the literature for viscous jets (see, e.g. Buckmaster, Nachman & Ting 1975; Entov & Yarin 1984; Ribe *et al.* 2006*a*). It shows the dependencies of the viscous stresses on the curvature of the fibre centreline.

REFERENCES

Antman, S. S. 2006 *Nonlinear Problems of Elasticity*. Springer.

Bechtel, S. E., Forest, M. G., Holm, D. D. & Lin, K. J. 1988 One-dimensional closure models for three-dimensional incompressible viscoelastic free jets: von Karman flow geometry and elliptical cross-section. *J. Fluid Mech.* **196**, 241–262.

Bishop, R. L. 1975 There is more than one way to frame a curve. *Am. Math. Monthly* **82** (3), 246–251.

Buckmaster, J. D., Nachman, A. & Ting, L. 1975 The buckling and stretching of a viscida. *J. Fluid Mech.* **69** (1), 1–20.

Caroselli, R. F. 1999 Glass textile fibers. In *Man-Made Fibers, Science and Technology* (ed. H. F. Mark, S. M. Atlas & E. Cernia), vol. 3, pp. 361–389. Interscience.

Chiu-Webster, S. & Lister, J. R. 2006 The fall of a viscous thread onto a moving surface: a 'fluid-mechanical sewing machine'. *J. Fluid Mech.* **569**, 89–111.

Cummings, L. J. & Howell, P. D. 1999 On the evolution of non-axisymmetric viscous fibres with surface tension inertia and gravity. *J. Fluid Mech.* **389**, 361–389.

Decent, S. P., King, A. C. & Wallwork, I. M. 2002 Free jets spun from a prilling tower. *J. Engng Math.* **42**, 265–282.

Decent, S. P., Simmons, M., Parau, E., Wong, D., King, A. & Partridge, L. 2004 Liquid jets from a rotating orifice. In *Proceedings of the 5th International Conference on Multiphase Flow*, Yokohama, Japan.

Dewynne, J. N., Howell, P. D. & Wilmott, P. 1994 Slender viscous fibers with inertia and gravity. *Q. J. Mech. Appl. Math.* **47**, 541–555.

Dewynne, J. N., Ockendon, J. R. & Wilmot, P. 1992 A systematic derivation of the leading-order equations for extensional flows in slender geometries. *J. Fluid Mech.* **244**, 323–338.

Dewynne, J. N. & Wilmott, P. 1993 Slender axisymmetric fluid jets. *Math. Comput. Model.* **18** (10), 69–82.

Do Carmo, M. P. 1998 *Differentialgeometrie von Kurven und Flächen*. Vieweg.

Eggers, J. 1997 Nonlinear dynamics and breakup of free-surface flow. *Rev. Mod. Phys.* **69**, 865–929.

Eggers, J. & Dupont, T. 2001 Drop formation in a one-dimensional approximation of the Navier–Stokes equation. *J. Fluid Mech.* **262**, 205–221.

Entov, V. M. & Yarin, A. L. 1984 The dynamics of thin liquid jets in air. *J. Fluid Mech.* **140**, 91–111.

Finnicum, D. S., Weinstein, S. J. & Ruschak, K. J. 1993 The effect of applied pressure on the shape of a two-dimensional liquid curtain falling under the influence of gravity. *J. Fluid Mech.* **255**, 647–665.

Forest, M. G. & Wang, Q. 1994 Dynamics of slender viscoelastic free jets. *SIAM J. Appl. Math.* **54** (4), 996–1032.

Forest, M. G., Wang, Q. & Bechtel, S. E. 2000 1-D models for thin filaments of liquid crystalline polymers: coupling of orientation and flow in the stability of simple solutions. *Physics* D **99** (4), 527–554.

Forest, M. G. & Zhou, H. 2001 Unsteady analyses of thermal glass fibre drawing process. *Eur. J. Appl. Math.* **12**, 497–496.

Geyling, F. T. & Homsey, G. M. 1980 Extensional instabilities of the glass fiber drawing process. *Glass Technol.* **21**, 95–102.

Gospodinov, P. & Roussinov, V. 1993 Nonlinear instability during the isothermal drawing of optical fibers. *Intl J. Multiph. Flow* **19**, 1153–1158.

Götz, T., Klar, A., Unterreiter, A. & Wegener, R. 2008 Numerical evidence for the non-existencing of solutions of the equations describing rational spinning. *Math. Models Meth. Appl. Sci.* **18** (10), 1–16.

Howell, P. D. 1994 Extensional thin layer flows. PhD thesis, St. Catherine's College, Oxford.

Howell, P. D. & Siegel, M. 2004 The evolution of a slender non-axisymmetric drop in an extensional flow. *J. Fluid Mech.* **521**, 155–180.

Marheineke, N. & Wegener, R. 2007 Dynamics of curved viscous fibers with surface tension. *Berichte des Fraunhofer ITWM* **115**.

Matovich, M. A. & Pearson, J. R. A. 1969 Spinning a molten threadline. Steady-state isothermal viscous flows. *Ind. Engng Chem. Fundam.* **8** (3), 512–520.

Panda, S. 2006 The dynamics of viscous fibers. PhD thesis, Technische Universität Kaiserslautern.

Panda, S., Marheineke, N. & Wegener, R. 2008 Systematic derivation of an asymptotic model for the dynamics of curved viscous fibers. *Math. Meth. Appl. Sci.* **31**, 1153–1173.

Partridge, L., Wong, D. C. Y., Simmons, M. J. H., Parau, E. I. & Decent, S. P. 2005 Experimental and theoretical description of the break up of curved liquid jets in the prilling process. *Chem. Engng Res. Des.* **83** (11), 1267–1275.

Pearson, J. R. A. 1985 *Mechanics of Polymer Processing*. Elsevier.

Pearson, J. R. A. & Matovich, M. A. 1969 Spinning a molten threadline. Stability. *Ind. Engng Chem. Fundam.* **8** (3), 605–609.

Ribe, N. M. 2004 Coiling of viscous jets. *Proc. R. Soc. Lond.* A **2051**, 3223–3239.

Ribe, N. M., Habibi, M. & Bonn, D. 2006*a* Stability of liquid rope coiling. *Phys. Fluids* **18**, 084102.

Ribe, N. M., Lister, J. R. & Chiu-Webster, S. 2006*b* Stability of a dragged viscous thread: onset of 'stitching' in a fluid-mechanical 'sewing machine'. *Phys. Fluids* **18**, 124105.

Schultz, W. W. & Davis, S. H. 1982 One-dimensional liquid fibres. *J. Rheol.* **26**, 331–345.

Shah, F. T. & Pearson, J. R. A. 1972 On the stability of non-isothermal fibre spinning. *Ind. Engng Chem. Fundam.* **11**, 145–149.

Sierou, A. & Lister, J. R. 2003 Self-similar solutions for viscous capillary pinch-off. *J. Fluid Mech.* **497**, 381–403.

Stokes, Y. M. & Tuck, E. O. 2004 The role of inertia in extensional fall of viscous drop. *J. Fluid Mech.* **498**, 205–225.

Stokes, Y. M., Tuck, E. O. & Schwartz, L. W. 2000 Extensional fall of a very viscous fluid drop. *Q. J. Mech. Appl. Math.* **53** (4), 565–582.

Trouton, F. R. S. 1906 On the coefficient of viscous traction and its relation to that of viscosity. *Proc. R. Soc. Lond.* A **77**, 426–440.

Wallwork, I. M., Decent, S. P., King, A. C. & Schulkes, R. M. S. M. 2002 The trajectory and stability of a spiralling liquid jet. Part 1. Inviscid theory. *J. Fluid Mech.* **459**, 43–65.

Wong, D. C. Y., Simmons, M. J. H., Decent, S. P., Parau, E. I. & King, A. C. 2004 Break up dynamics and drop size distributions created from curved liquid jets. *Intl J. Multiph. Flow* **30**, 499–520.

Yarin, A. L. 1993 *Free Liquid Jets and Films: Hydrodynamics and Rheology*. Longman.

Yarin, A. L., Gospodinov, P., Gottlieb, O. & Graham, M. D. 1999 Newtonian glass fiber drawing: chaotic variation of the cross-sectional radius. *Phys. Fluids* **11** (11), 3201–3208.